Review | Open Access

Engin Future

Wang *et al. Engin Fut.* **2026**, *1*, 4 **DOI:**10.20517/enginfuture.2026.03

# The precise synthesis of etched metal-organic frameworks and their applications in electrochemistry

**Sitong Wang[1], Jiayi Fan[1], Sijin Li[1], Mohsen Shakouri[2], Rongmei Zhu[1,*]**

**Keywords:**
Metal-organic framework, etching approach, electrolysis, energy storage

**Citation:** Wang, S.; Fan, J.; Li, S.; Shakouri, M.; Zhu, R. The precise synthesis of etched metal-organic frameworks and their applications in electrochemistry. *Engin Fut.* **2026**, *1*, 4. https://dx.doi.org/10.20517/enginfuture.2026.03

**Received:** 8 May 2026
**First Decision:** 22 Jun 2026
**Revised:** 6 Jul 2026
**Accepted:** 26 Aug 2026
**Published:** 23 Sep 2026

**Academic Editor:**
Uk Sim
**Copy Editor:**
Shu-Yuan Duan
**Production Editor:**
Shu-Yuan Duan

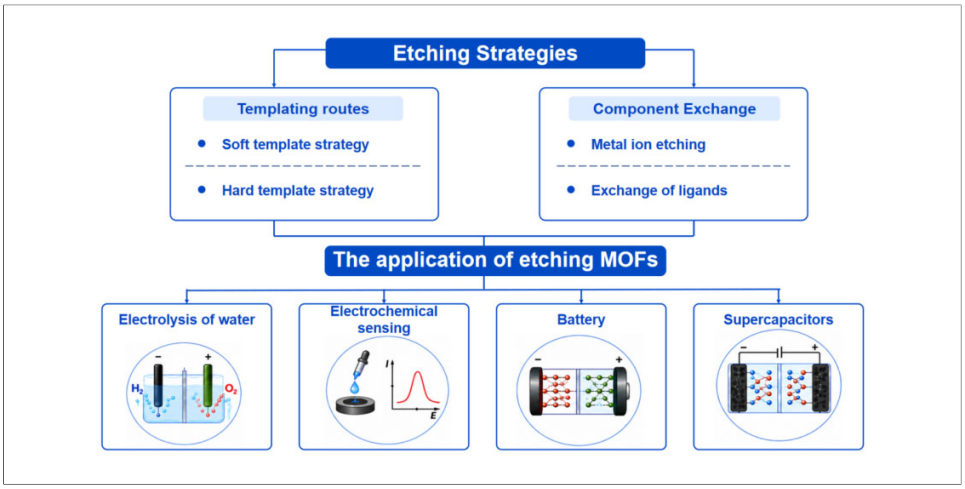


## Abstract

Metal-organic frameworks (MOFs) have garnered extensive utilization across chemical, biomedical, and energy-related disciplines owing to their exceptional specific surface area and tunable structural features. Nevertheless, the electrical conductivity and long-term durability of conventional MOF materials remain inadequate for many advanced applications. Etching approaches offer a promising route to generate additional defect sites and catalytic centers within MOF architectures and their derivatives, thereby significantly expanding their functionality in electrochemical systems. This review systematically elaborates on various etching techniques, encompassing hard- and soft-templating routes, metallic ion etching, and ligand exchange protocols. It further highlights the performance of etched MOFs in electrocatalytic processes, supercapacitors, and battery technologies. Prospects for future development and prevailing challenges in the field of etched MOF materials are also critically discussed.



[1]School of Chemistry and Materials, Yangzhou University, Yangzhou 225002, Jiangsu, China.
[2]Canadian Light Source, University of Saskatchewan, Saskatoon, Saskatchewan S7N 2V3, Canada.

[*]**Correspondence to:** Prof. Rongmei Zhu, School of Chemistry and Materials, Yangzhou University, Yangzhou 225002, Jiangsu, China. E-mail: rmzhu@yzu.edu.cn

## INTRODUCTION

The escalating global energy demand and the accelerating depletion of conventional fossil resources have precipitated severe environmental challenges. In response, the development of clean and renewable energy alternatives, such as solar, wind, tidal, and hydrogen energy, has become an imperative strategy to mitigate reliance on traditional carbon-based fuels[1]. Within this context, metal-organic frameworks (MOFs) have emerged as a class of materials with significant potential for energy applications[2]. Comprising metal nodes interconnected by organic ligands through coordination bonds, MOFs represent a distinctive family of porous crystalline materials that have attracted considerable attention over the past twenty years[3-5]. In contrast to conventional porous solids, MOFs exhibit exceptional characteristics, including ultrahigh surface areas, tunable pore geometries, and scalable, green synthetic feasibility with mild reaction conditions and recyclable raw material options. Such tunable synthesis further facilitates large-scale pilot preparation of MOF precursors at reduced production cost. These attributes render them highly promising for a diverse range of applications, spanning gas adsorption and storage, molecular sensing, drug delivery, and catalytic processes[6].

The synthesis and properties of MOFs are strongly influenced by the selection of metal ions, organic linkers, and functional modifiers[7,8]. Notably, even identical precursor combinations can yield distinct structural configurations and material characteristics, underscoring the critical role of synthetic control[9]. Variations in synthesis methods and reaction conditions further modulate morphology, crystallinity[10-12], and porosity, thereby directly determining the functional performance of the resulting materials[13]. Despite their advantages in porosity and tailorability, MOFs often suffer from intrinsic limitations such as poor electrical conductivity[14], limited chemical resilience, particularly under acidic conditions due to the labile nature of coordination bonds and insufficient mechanical robustness[15,16]. These shortcomings significantly restrict their applicability, especially in electrochemical systems[17]. Moreover, the predominantly microporous nature (pores < 2 nm) of conventional MOFs imposes diffusion constraints, narrowing their utility in composites and processes requiring rapid mass transport[18,19].

As a result, strategies such as composite formation, ligand exchange, and etching have been developed[20,21]. Among these, etching techniques have proven particularly effective in engineering hierarchical porosities and exposing abundant active sites while largely preserving the innate high surface area and structural integrity. The resulting etched MOFs exhibit significantly enhanced functionality, opening new avenues for advanced applications[22].

The term "active site" should be defined according to the chemical identity and coordination environment of the species directly involved in adsorption, electron transfer, ion storage, or bond activation. In pristine MOFs, many metal centers are coordinatively saturated by organic linkers, and their accessibility to reactants is restricted by the surrounding coordination environment. Selective cleavage of metal-linked bonds during etching can convert these initially saturated nodes into chemically distinct sites, including missing-linker-adjacent metal centers, missing-node-associated defect regions, coordinatively unsaturated metal sites, exposed linker termini, defect-compensating hydroxyl or water ligands, and reconstructed metal-containing edge sites.

MOF etching is defined here as a post-synthetic subtractive modification process in which selected framework constituents or spatial domains of a preformed MOF are removed through controlled chemical reactions, thereby generating defects, enlarged pores, altered facets, or internal cavities while retaining at least part of the material as a chemically identifiable MOF phase. Accordingly, removal of an externally introduced sacrificial template is referred to as de-templating or template-assisted hollowing, whereas processes involving extensive dissolution of the MOF and simultaneous formation of layered double hydroxides (LDHs), oxides, sulfides, phosphides, or carbon materials are described as etching-coupled reconstruction.

Recent studies highlight the considerable potential of chemical etching in modulating both the functionality and microstructure of MOFs[23,24]. This review comprehensively examines etching strategies aimed at enhancing the electrochemical performance of MOFs[25]. These approaches can be categorized according to the use and nature of templates[26,27], such as hard or soft templates, or by the targeting of

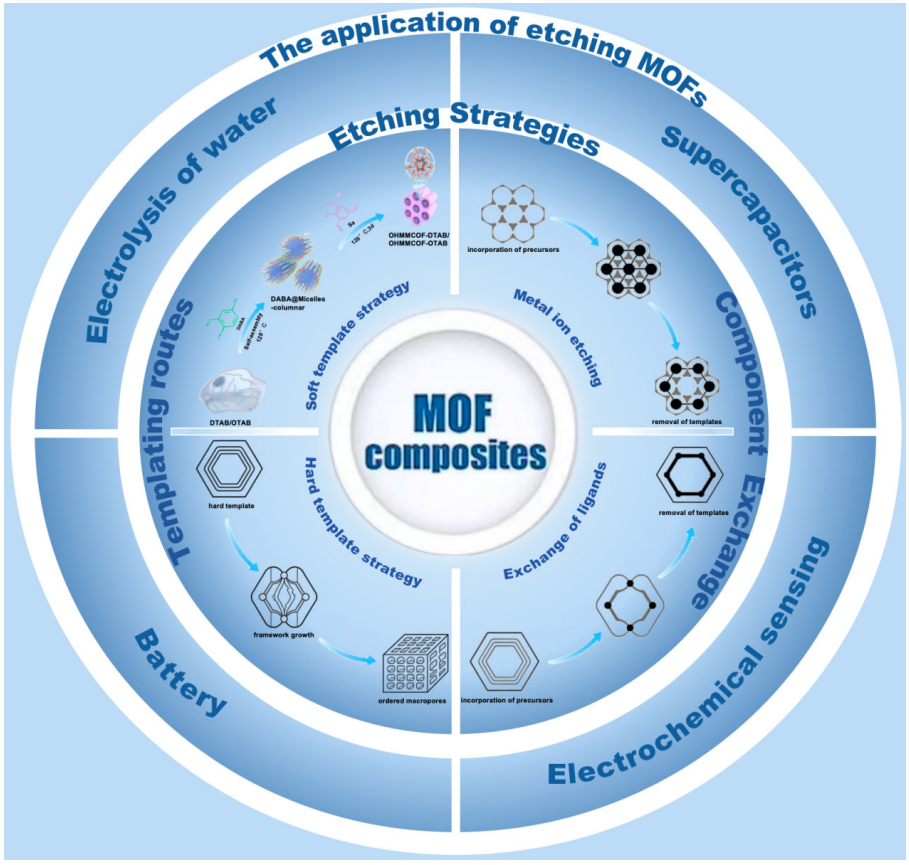


**Figure 1.** Summary of etching strategies. Soft template strategy (upper left); This figure is adapted from Ref.[30]. Copyright 2024. Licensed under CC BY 4.0. MOF: Metal-organic framework; DABA: 2,5-diaminobenzenesulfonic acid; DTAB: Dodecyltrimethylammonium bromide; OTAB: Octadecyltrimethylammonium bromide.

specific components. MOF etching is defined as a typical post-synthetic structural engineering, including metal nodes and organic ligands[28]. We critically evaluate the merits and limitations of each etching strategy, systematically summarize recent breakthroughs in the electrochemical applications of etched MOFs [Figure 1], and offer perspectives on future research directions and challenges in this evolving field[29].

Distinct from previously published review papers focusing on general post-synthetic modification or single-type hollow MOF preparation, this review establishes a novel etching classification standard based on the intrinsic coordination bond cleavage mechanism rather than superficial preparation routes: template-directed etching, metal-node selective etching and ligand cleavage/swap etching are systematically categorized and elaborated, which is absent in most existing relevant summaries. Meanwhile, different from prior reviews covering gas separation, photocatalysis and multi-disciplinary applications together, our work tightly restricts all application discussions into four core electrochemical fields: electrocatalytic water splitting, supercapacitor electrodes, rechargeable batteries and electrochemical sensing, and quantitatively correlates etching parameter-structure-electrochemical performance for each category of etched MOFs[30]. Besides, we summarize numerous newly developed mild green etching strategies reported after 2021 that have not been comprehensively reviewed yet, including tannic acid selective core protection etching, dual Lewis acid-electrochemical co-etching and dry gaseous thiourea ligand etching, further highlighting the unique summarizing perspective of this manuscript.

Additionally, one common academic skepticism toward MOF etching research is that expensive high-purity organic ligands are consumed for pristine MOF synthesis followed by partial framework removal via etching, leading to potential raw material waste[31]. Nevertheless, three irreplaceable

research merits justify the continuous exploration of MOF etching: firstly, precise partial etching maximizes the utilization efficiency of costly organic components by creating abundant accessible active sites without discarding the whole MOF skeleton; secondly, etching is a low-cost post-modification approach to fabricate hierarchical porous electroactive architectures that cannot be directly synthesized via one-pot solvothermal with cheap precursors; thirdly, etched MOF derivatives show greatly improved cyclic stability in harsh electrochemical electrolyte, realizing long-term cyclic reuse of expensive metal-ligand resources. Based on the above unique classification, exclusive electrochemical orientation and practical research value, this review systematically summarizes the state-of-the-art progress of precision-etched MOFs for electrochemical applications.

## METHODS OF ETCHING MOFS

In recent years, numerous synthesis strategies for MOFs have been developed, including conventional solvothermal routes, template-assisted growth, and ultrasound-assisted preparation[32,33]. Despite these advances, the inherently narrow pore size distribution of many MOFs often restricts their efficiency in energy storage applications[34,35]. Rational modulation of the pore architecture represents a critical pathway to overcome this limitation[36]. Chemical etching, which operates through selective cleavage of coordination bonds between metal ions and organic ligands, has emerged as an effective means to tailor pore characteristics[37]. MOF etching refers to a post-synthetic structural modification method that selectively breaks partial metal-ligand coordination bonds to remove partial components from MOF frameworks without full crystalline collapse, producing hierarchical pores, hollow cavities or abundant unsaturated active sites. Precise control over etching parameters is essential to achieving desired structural properties[38], including porosity, morphology, crystal facet exposure, and chemical composition[39]. This section outlines three principal etching approaches: template method, metal ion exchange and ligand exchange[40,41].

MOF etching is defined as a typical post-synthetic structural engineering technology[42] that selectively cleaves partial metal-organic coordination bonds via chemical/physical etching agents, selectively removing partial foreign template cores, intrinsic metal node sites or organic ligand segments from parent MOF, to construct hierarchical pores, hollow cavities or coordinatively unsaturated surface active sites while preserving the overall crystalline backbone of original MOF. All three core strategies (hard/soft template etching, metal ion etching, ligand exchange etching) fall within the scope of MOF etching, with classification differentiated by the specific etched object: template etching eliminates externally introduced sacrificial template substances embedded during MOF in-situ growth; metal ion etching targets selective dissolution or ion replacement of intrinsic metal coordination nodes on MOF skeleton; ligand-oriented etching achieves framework reconstruction via breaking and substituting partial original organic linkers. Based on this unified definition and classification logic, we elaborate three mainstream etching pathways in detail below.

### Template method

Based on the nature of the templating materials, template-based synthesis strategies can be categorized into hard-templating and soft-templating approaches[43,44]. Hard/soft templating etching removes embedded sacrificial template substances inside MOF crystals after framework growth. An ideal template should combine ease of preparation with controlled etchability, thereby enabling the precise preservation of the desired MOF architectures and morphological features.

#### *Hard template strategies*

Hard templates, including $SiO_2$, metals, and polymers, typically exhibit well-defined and tunable geometries that facilitate the formation of core-shell architectures. Subsequent removal of the core template allows the preservation of the shell's original morphology[45]. The fabrication of hollow MOFs via hard-templating generally involves three key steps: first, synthesis of a template with specific shape and dimensions; second, controlled growth of the MOF shell over the template surface; and finally, removal of the core to yield hollow structures[46]. For instance, Wang *et al.* constructed nitrogen-doped carbon hollow microtubules (denoted as N-GCT) using ZnO nanorods as a sacrificial template in a ZnO@zeolitic imidazolate framework-8 (ZIF-8) system [Figure 2][47]. Their study revealed that the shell thickness could be precisely modulated by varying

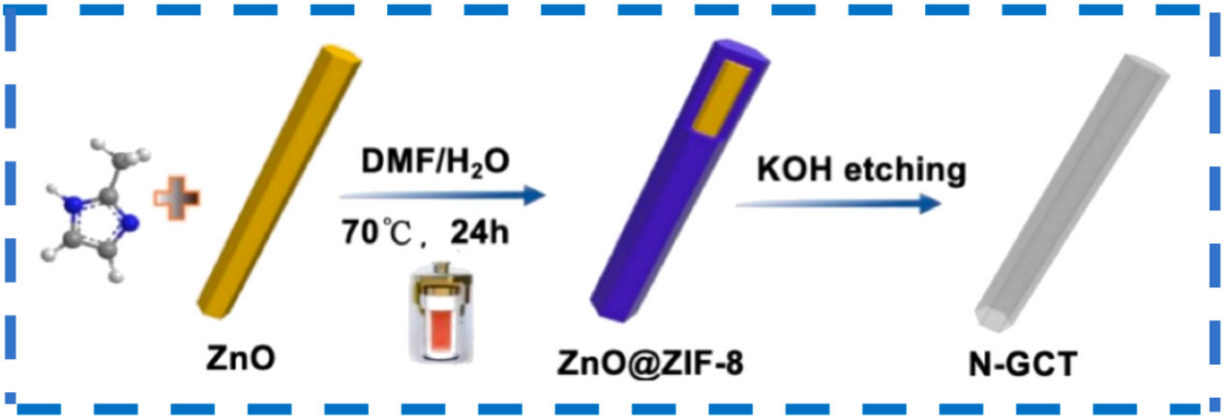


**Figure 2.** Schematic representation of the preparation of N-GCT; This figure is adapted from Ref.[47]. Copyright@2022, Youke Publishing. DMF: N,N-dimethylformamide; ZIF: zeolitic imidazolate framework; N-GCT: nitrogen-doped carbon hollow microtubule.

the reaction time or temperature. After etching with KOH, the resulting N-GCT retained a well-defined hollow architecture without structural collapse, and exhibited high specific surface area and pore volume, resulting in enhanced performance as a cathode material in lithium-sulfur batteries.

Beyond conventional metal oxide templates, MOFs have been employed as sacrificial templates to fabricate hollow polyhedral architectures[48,49]. The surfactant cetyltrimethylammonium bromide (CTAB) was critical in selectively inhibiting the growth of the (100) crystal facets, promoting the formation of a well-defined cubic architecture[50]. This enabled the subsequent formation of ZIF-67/Co-Fe Prussian blue analog (PBA) multilayer nanoboxes. Finally, during annealing, the ZIF-67 template was etched away, resulting in hollow nanoboxes with maintained structural integrity.

Among various hard-template options, polystyrene (PS) spheres are widely utilized for constructing hollow MOFs and MOF-based composites owing to their mild synthesis and removal conditions[51]. Carboxyl groups on the PS surface facilitate zinc ion coordination, promoting heterogeneous nucleation and growth of ZIF-8 on the template. Subsequent immersion selectively removes the PS core, yielding intact hollow microspheres[52]. By precisely controlling the growth cycles, the ZIF-8 shell thickness can be finely tuned, enabling optimization of the material's physicochemical and functional properties[53]. Furthermore, the versatility of PS templates allows the engineering of more complex architectures, such as hollow double-shell MOF structures through iterative templating strategies.

Despite its utility in fabricating hollow MOFs, the hard-template method encounters several challenges during the etching process. These include difficulty in completely removing the template, limited structural stability of the resulting MOFs, imprecise control over pore size distribution, and overall procedural complexity[54]. In contrast, soft-templating strategies offer notable advantages: milder template removal conditions, finer regulation of pore architecture, improved structural integrity of the MOFs, and a more streamlined synthesis process[55]. These characteristics make soft-template etching particularly suitable for constructing MOFs with hierarchical porosity, well-defined hollow morphologies, and tailored functionality[56].

### *Soft template strategy*

Surfactants, by virtue of their amphiphilic nature, self-assemble into micelles or vesicles in solution, serving as soft templates to direct the formation of tailored nanostructures[57]. Surfactants like sodium dodecyl sulfate (SDS) and alkyltrimethylammonium bromide ($C_n$TAB) are particularly effective for crafting hollow MOFs through etching strategies[58,59]. Electrostatic interactions and hydrogen bonding facilitate the crystallization of MOFs on the surfactant surfaces, while morphological control can be achieved by tuning surfactant concentration, reaction temperature, and pH[60,61].

Beyond anionic systems, cationic soft templates such as $C_n$TAB vesicles have also been employed[62,63]. Zhang *et al.* demonstrated that upon mixing $C_n$TAB with $Co(NO_3)_2$ and HmIM in aqueous solution, negatively charged [Co-complex]$^-$ species adsorb onto the cationic vesicle surface, providing nucleation sites for ZIF-67 crystallization. Subsequent washing with N,N-dimethylformamide (DMF) and methanol etches away the soft template, resulting in hollow ZIF-67 particles with uniform structural integrity[64].

## Exchange of metal ions

A wide variety of MOFs with diverse compositions and structural features have been extensively investigated. Key strategies for tailoring MOF architectures include central metal ion exchange, ligand etching and substitution, defect engineering, template-guided assembly, and ligand functionalization. While extending the length of organic linkers can facilitate the formation of mesopores of varying sizes, it often compromises the framework stability due to reduced coordination connectivity[65]. Among these approaches, etching and exchanging central metal ions represent one of the most straightforward routes to structural modification[66]. Exchange of metal ions selectively dissolves or replaces intrinsic metal centers of the parent MOF skeleton via acid or competing metal ions. These processes not only alter the chemical composition but also enable precise control over morphology and crystalline orientation. Commonly employed metal ion etching techniques involve proton acid etching and competitive metal ion displacement, which typically target specific crystal facets or sites to create enlarged mesopores or customized morphological features[67,68].

Acid etching serves as a highly effective route for constructing hierarchical porous MOF architectures. By selectively cleaving coordination bonds between metal nodes and organic ligands using proton acids, this method enables precise control over MOFs' morphology[69], facilitating the creation of hollow and highly porous structures. Tannic acid forms a protective coating on the external surface, while the released protons diffuse into the framework and protonate the N-donor sites of the 2-methylimidazolate linkers[70]. This protonation decreases the electron-donating ability of the linkers and progressively weakens the Co-N coordination bonds, leading to preferential dissolution of the internal framework and the formation of hollow ZIF-67-derived structures. Liu *et al.* developed a synergistic protection etching strategy to fabricate hollow ZIF-67 polyhedra and carbon nanocages (Co@NCNs) displayed in Figure 3A, circumventing the limitations of conventional sacrificial templates and strong etchants[71]. Tannic acid (TA), rich in hydroxyl groups, was coated on ZIF-67 surfaces. Protons released from TA diffused inward through pores, selectively breaking Co-N bonds and inducing core-selective etching, with shell thickness finely adjustable via etching duration[72]. Liu *et al.* demonstrated multi-shell hollow MIL-101(Cr) with single-crystal shells through stepwise crystal growth and acetic acid etching [Figure 3B][73]. The differential stability between outer and inner layers allowed selective etching, with cavity size and shell thickness modulated by etching time and reactant concentration.

The Ting group utilized phosphoric acid to selectively etch the metastable HKUST-1, generating a defect-rich porous copper-based MOF with hexagonal macroporosity while preserving crystallinity[74]. Their experiments confirmed etching dependence on both time and acid concentration. As shown in Figure 3C, Cai *et al.* employed cyanuric acid (CA) to anisotropically etch ZIF-67 truncated rhombic dodecahedra[75]. CA preferentially passivated the (100) facets, enabling inward excavation of the six equivalent crystal planes, ultimately yielding well-defined hollow nanoframes.

Beyond proton acid etching, the use of excess metal ions represents another prevalent strategy for modifying MOF structures. This approach operates on the principle of selective coordination differences, where the etching agent must exhibit a coordination affinity toward the organic ligand that is comparable to or greater than that of the native metal ions within the MOF framework. This method yielded a bimetallic MOF with high crystallinity and no detectable impurity phases. Zeng *et al.* developed a bifunctional etching strategy for ZIF-67 that avoids organic acids entirely[76]. This dual-functional approach combines structural etching with in situ active-site loading. In a related study, Ulisso *et al.* employed a cationic etching method to transform ZIF-67 into hierarchical perovskite $LaCoO_3$ incorporated with spinel $Co_3O_4$ polycrystals[77].

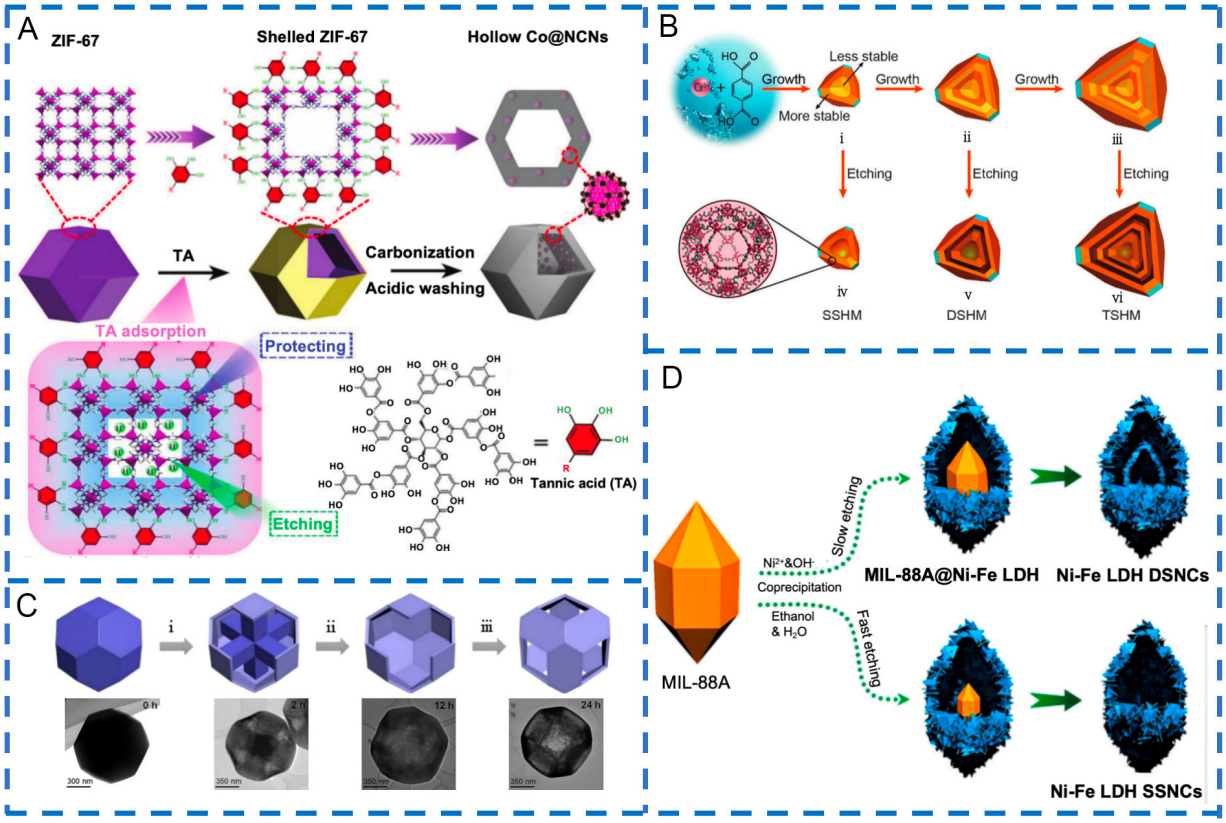


**Figure 3.** The schematic illustration for the synthetic procedure of (A) hollow Co@NCNs; This figure is adapted from Ref.[71]. Copyright@2021, Wiley-VCH; (B) single-, double-, and triple-shelled hollow MIL-101; This figure is adapted from Ref.[73]. Copyright@2017, Wiley-VCH; (C) tZIF-67 hollow nano-frame and the corresponding TEM images; This figure is adapted from Ref.[75]. Copyright@2021, Wiley-VCH; (D) Schematic illustration of preparing Ni-Fe LDH nanocages with tunable shells. This figure is adapted from Ref.[87]. Copyright@2021, Wiley-VCH. ZIF: Zeolitic imidazolate framework; TA: tannic acid; SSHM: Single-shelled hollow microcage; DSHM: Double-shelled hollow microcage; TSHM: Triple-shelled hollow microcage; DSNC: Double-shelled nanocage; SSNC: Single-shelled nanocage; MIL: Materials of the Institute Lavoisier; NCN: N-doped carbon nanosheets / Nitrogen-doped carbon network; LDH: layered double hydroxide.

LDHs belong to a class of anionic layered materials characterized by brucite-like sheets in which metal cations occupy octahedral sites coordinated by hydroxyl groups[78]. Owing to their tunable chemical composition, ion-exchange capability, high intrinsic stability, and rich redox properties, LDHs exhibit outstanding performance across various applications[79]. Recently, metal ion etching has been widely adopted for synthesizing LDHs with hierarchical structures from MOF precursors, significantly enhancing the electrochemical utility of MOF-derived materials[80,81]. Competitive metal-ion etching involves simultaneous dissolution of the original metal nodes and formation of new coordination environments. During the conversion of ZIF-67 or Co-ZIF-L into NiCo-based layered double hydroxides, incoming $Ni^{2+}$ or $Co^{2+}$ ions and hydrolyzed hydroxide species interact with the framework surface[82]. The hydrolysis-induced weakening of the original Co-N coordination bonds promotes the release of imidazolate linkers and Co-containing species, while the incoming metal ions are subsequently re-coordinated with OH- to nucleate NiCo-LDH nanosheets. For example, Guan *et al.* constructed bimetallic NiCo-LDH polyhedra through $Co^{2+}$ and $Ni^{2+}$ etching of ZIF-67[83]. The bimetallic system promotes the formation of numerous ultra-thin, vertically aligned LDH nanosheets assembled into hollow polyhedral superstructures in contrast to monometallic Co-LDH. This unique configuration maximizes interfacial exposure and facilitates guest-host interactions, thereby enhancing electrochemical activity. The Co-ZIF-L was first etched with $Co^{2+}$ in a DMF-ethanol solution, followed by further $Ni^{2+}$-assisted etching, yielding a material labeled CoNi-1 that demonstrated superior electrochemical performance[84,85].

Furthermore, the shell architecture of hollow LDHs,

including shell number and hierarchy, can be precisely tailored by modulating etching conditions[86]. As demonstrated by Zhang *et al.*, adjusting the ethanol-to-water ratio during etching allows fine control over reaction kinetics[87]. With higher ethanol content, etching is slowed, leading to the formation of double-shelled Ni-Fe LDH nanocages (DSNCs), as illustrated in Figure 3D. In contrast, aqueous-rich conditions favor single-shelled structures. This involves etching-coupled dissolution and reprecipitation, in which a new active phase is generated during the etching process itself. The conversion of ZIF-67 or Ni-MOF into NiCo-LDH is a representative example[88,89]. Incoming metal ions and hydrolyzed hydroxide species cleave the original metal-imidazolate coordination bonds while simultaneously nucleating LDH nanosheets. The increased capacitance or catalytic activity therefore arises from two coupled changes: the hollow or hierarchical morphology inherited from selective dissolution, and the formation of a redox-active NiCo-LDH phase containing Ni and Co centers capable of reversible valence transitions. In this situation, etching and phase transformation are chemically inseparable steps. It is more accurate to state that etching directs the reconstruction and spatial organization of the active LDH phase, rather than claiming that etching alone produces the electrochemical enhancement.

Building upon the complementary strengths of proton acid etching, which enables hollow structure formation and transition metal ion etching that allows crystal structure regulation, the integration of both strategies offers a powerful route for fabricating anisotropic materials with finely tunable composition and architecture[90]. Liu *et al.* demonstrated this synergistic approach by simultaneously employing transition metal and protic acid etching to synthesize hollow carbon polyhedra[91]. In their method, $Ni^{2+}$ ions first etched ZIF-67 to form a NiCo@LDH intermediate, which was subsequently treated with boric acid ($H_3BO_3$) to selectively etch the framework, resulting in well-defined hollow structures with maintained polyhedra morphology[91].

## Exchange of ligands

Beyond metal ion etching, etching and exchange represent another effective approach for structural and compositional modulation of MOFs[92]. Exchange of ligands replaces or strips partial original organic linkers by strong bases or competing coordinating molecules. This strategy readily yields hollow architectures and novel chemical functionalities. Alkaline agents or strongly coordinating ligands are typically employed as etchants to selectively remove or replace original linkers, thereby creating porous frameworks or inducing phase transformations[93].

For example, Li *et al.* demonstrated alkaline etching of a copper-based MOF (Cu-MOF-74) to synthesize hollow copper sulfides with tunable morphologies. Ligand-oriented etching proceeds through the preferential cleavage or substitution of the original metal-linker coordination bonds by hydroxide ions, competing anions, or thermally generated reactive species. The alkaline transformation of Cu-MOF-74 illustrates this process. During KOH treatmen[94], OH- coordinates with the Cu centers and promotes hydrolysis and dissociation of the original Cu-O bonds formed between $Cu^{2+}$ and the carboxylate linkers. This gradual decoordination enables a pseudomorphic structural transformation while largely retaining the external particle morphology. Subsequent treatment with $Na_2S$ replaces the original O-donor coordination environment with stronger Cu-S interactions, leading to further removal of the organic framework and the formation of hollow copper sulfides. Thus, the observed rod-to-cube-to-dodecahedron evolution reflects the balance between alkaline cleavage of Cu-O bonds, framework reconstruction, and sulfide-induced coordination substitution. Subsequent sulfidation yielded the corresponding hollow sulfide derivatives[95]. Hydroxide ions generated from ammonia cleavage selectively removed the inner $Co(CN)_6^{3-}$ ligands, resulting in structurally defined hollow frameworks. Hydroxide ions generated from $NH_3{\cdot}H_2O$ preferentially attack accessible metal-cyanide coordination units, weakening the Co-C≡N-Co bridges and promoting the dissolution of internal $[Co(CN)_6]^{3-}$ units. Because the corners and edges possess lower coordination numbers and higher accessibility than the planar regions, ligand removal begins preferentially at these positions, producing hollow or open-frame intermediates. Subsequent chalcogenide-ion exchange reconstructs the residual metal centers into Cu-$CoSe_2$ nanoframes. At 650 °C, thiourea decomposition releases $H_2S$, which serves as a gaseous etchant enabling sulfide formation through

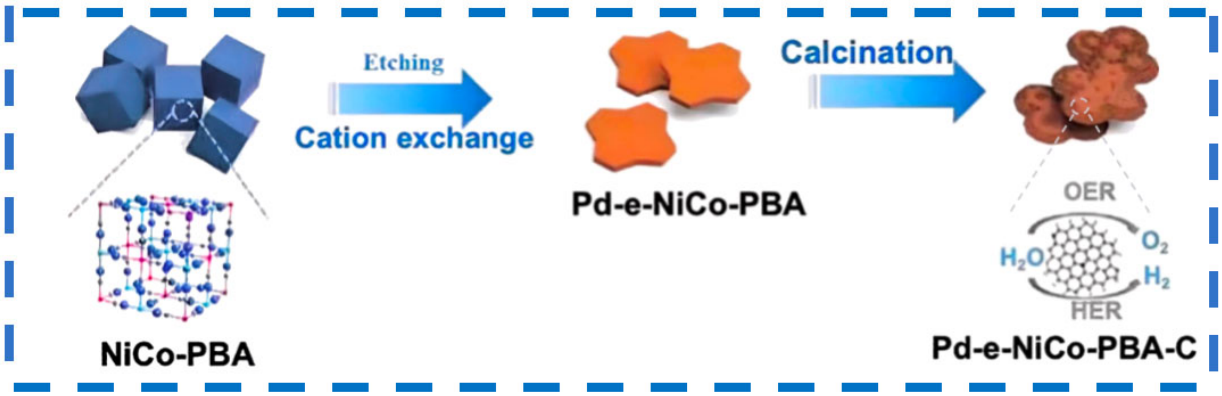


**Figure 4.** Schematic illustration of preparing Pd-e-NiCo-PBA-C; This figure is adapted from Ref.[96]. Copyright@2021, licensed under CC BY 4.0. NiCo-PBA: NiCo Prussian blue analogue; Pd-e-NiCo-PBA: Pd-etched NiCo Prussian blue analogue; OER: oxygen evolution reaction; Pd-e-NiCo-PBA-C: Pd-etched NiCo Prussian blue analogue-derived carbon.

**Table 1. Quantitative comparison of etching behavior among representative MOF families**

| MOF family | Representative MOF | Etchant /medium | Etching conditions | Etching product | Ref. |
|---|---|---|---|---|---|
| ZIF | tZIF-67 | Cyanuric acid | 12 h | Hollow ZIF-67 nanoframe | [76] |
| UiO | UiO-66-$(OH)_2$ @UiO-66-Br | $HNO_3$ | 24 h | Hollow UiO-66 | [127] |
| UiO | UiO-66-$(OH)_2$ @UiO-66-Br | $SO_4^{\cdot-}$/·OH | 1.5 h | Hollow UiO-66 | [128] |
| HKUST | HKUST-1 | $H_3PO_4$/ DMSO-MeOH | pH 2.6, 40 °C, 72 h | Macroporous defect-rich HKUST-1 | [75] |
| HKUST | HKUST-1 | $H_3PO_4$/ DMSO-MeOH | pH 2.6, 40 °C, 240 h | Highly etched macroporous HKUST-1 | [75] |

MOF: Metal-organic framework; ZIF: zeolitic imidazolate framework; DMSO: dimethyl sulfoxide; HKUST: Hong Kong University of Science and Technology.

reaction with $Fe^{3+}$ nodes.

Zhang *et al.* further developed an ammonia-assisted *in situ* cation exchange method to fabricate dodecagonal N-doped carbon nanosheets (Pd-e-NiCo-PBA-C) [Figure 4][96]. Unlike conventional cubic hollow structures, this unique skeletal framework resulted from anisotropic etching initiated at the vertices of the precursor cube, evolving progressively into a cage-like architecture and ultimately a hollow morphology, exhibiting exceptional electrocatalytic performance in water splitting.

To better reveal the etching behavior on representative MOFs, a quantitative comparison is listed in Table 1.

## TCHING MOF-DERIVED HETEROSTRUCTURES

The morphology of MOFs can be categorized into one-dimensional forms such as nanorods and nanobelts, two-dimensional nanosheets, and three-dimensional architectures including nanoflowers and polyhedra[97]. Through etching strategies, both MOFs and their derivatives can be engineered into advanced configurations, such as hollow, core-shell, and ring-shaped structures that extend beyond their original frameworks. These modified materials not only retain the inherent structural advantages of MOFs but also facilitate enhanced charge transfer across multi-component interfaces, significantly boosting electrochemical performance[98]. This section will focus particularly on two prominent etched architectures: core-shell and hollow structures.

## Core-shell structure

Core-shell nanostructures constitute a significant class of nanomaterials characterized by a distinct core enveloped by a surrounding shell[99]. Broadly speaking, they comprise ordered architectures formed through the encapsulation of one nanomaterial by another via chemical bonds or physical interactions, encompassing both conventional core-shell configurations and yolk-shell structures that incorporate an interstitial void between core and shell[100].

In the context of MOF-based core-shell systems, structural design has evolved from relatively simple forms to increasingly complex architectures. The shell serves a critical protective role, shielding the core from the external environment and providing a confined space that enhances reaction stability. When the shell is composed of porous MOFs, it further facilitates molecular transport by offering additional pore channels, shortening diffusion pathways, promoting electrolyte infiltration, especially in hollow configurations and enhancing charge and mass transfer kinetics[101,102]. Moreover, the synergistic interplay between core and shell components enables the integration of multifunctional properties, substantially broadening the application potential of these materials across catalytic, energy storage, sensing, and biomedical fields[103].

Shell thickness and shell number are particularly important kinetic parameters. A thin porous shell shortens the solid-state ion-diffusion distance and provides rapid access to internal active sites, whereas an excessively thin shell may collapse during cycling or lose electrical continuity. Multishell structures provide a larger electrode-electrolyte interfacial area and multiple diffusion channels, but overly compact or poorly connected shells may increase ion-transport resistance.

Single-layer core-shell structures are commonly fabricated via self-templating methods, which enable precise control over dimensions and morphological uniformity[104]. In contrast to conventional hard- or soft-templating approaches, self-templating not only ensures well-defined core-shell architectures but also allows tailored regulation over MOF composite properties. Among various synthetic routes, the one-pot method represents a straightforward and efficient strategy, wherein metal precursors and organic ligands are simultaneously introduced into a reaction system to achieve in situ core encapsulation and shell formation with narrow size distribution[105,106]. Initially, polyvinylpyrrolidone (PVP)-stabilized CdS NPs were synthesized, followed by controlled growth of a ZIF-8 shell onto the CdS surface. By varying the concentration of the 2-methylimidazole precursor, the thickness of the ZIF-8 shell could be precisely tuned from 102 ± 5.4 nm down to 13.6 ± 2.5 nm[107].

Magnetic $Fe_3O_4$ nanoparticles were sequentially immersed in ethanolic solutions containing the zirconium cluster precursor $Zr_6O_4(OH)_4^{12+}$ and the organic linker 2-aminoterephthalic acid, with magnetic separation after each step, to achieve uniform MOF encapsulation. In contrast to conventional chemical etching, water etching offers an environmentally benign and cost-effective route for generating highly porous yolk-shell structures without aggressive reagents[108].

From a structural perspective, MOF-derived core-shell architectures can be classified into two primary categories: single-shell and multi-shell systems. Unlike their single-shell counterparts, multi-shell heterostructures incorporate multiple concentric or hierarchical layers, offering enhanced compositional complexity and tailored functionality[108]. These sophisticated architectures can be synthesized through self-templating strategies, often coupled with selective etching or ion-exchange processes. For example, Cao *et al.* fabricated hollow spherical structures starting from solid NiCo metal glycerate spheres[109].

Alternatively, carbon-rich MOFs prepared via solvothermal methods exhibit exceptional metal cation permeability, enabling the construction of multi-shell hollow structures through post-synthetic modification. Guan *et al.* illustrated this approach by first synthesizing Mn-Co coordination polymer spheres through solvothermal reaction of $Mn^{2+}$ and $Co^{2+}$ with isophthalic acid ($H_2IPA$)[110]. The resulting precursor was subsequently calcined to form multi--shell bimetallic oxide particles and then phosphatized using $NaH_2PO_2$ to yield multi-shell Mn-Co oxyphosphide, as depicted in Figure 5.

## Hollow structure

Hollow nanostructured materials possess a range of

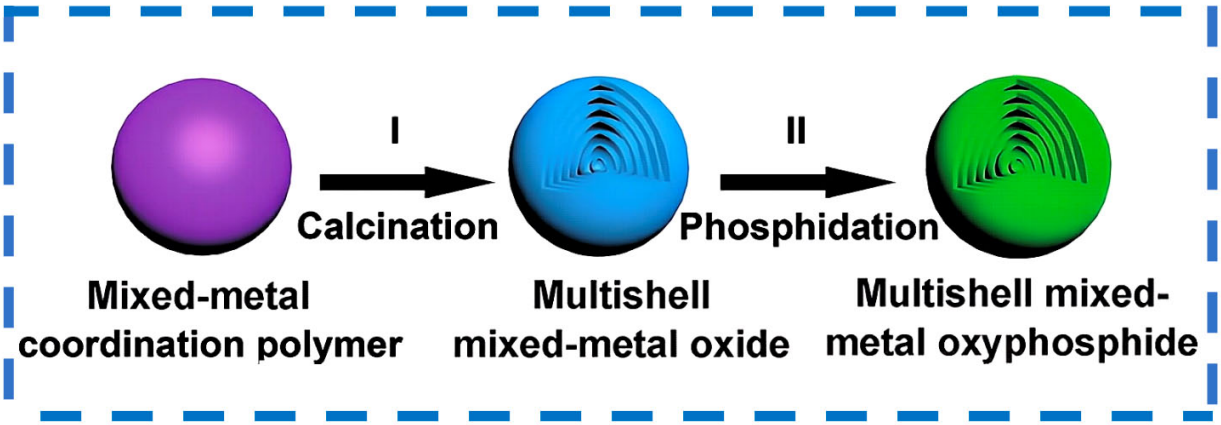


**Figure 5.** Schematic preparation of multishell mixed-metal oxyphosphide particle; This figure is adapted from Ref.[110]. Copyright@2017, Wiley-VCH.

advantageous properties, including high specific surface area for enhanced mass diffusion, abundant exposed active sites adaptable to diverse applications, and substantial internal void space enabling high loading capacity[111]. Etched MOFs with hollow architectures further benefit from tunable surface chemistry, enlarged pore size, and elevated surface area[112]. Notably, their hollow morphology facilitates rapid electrolyte penetration and efficient gas release compared to solid counterparts, contributing to their widespread use and high performance across numerous applications.

Two primary strategies are employed for fabricating hollow MOFs and their derivatives: template-assisted and post-processing methods. In the template-assisted approach, hollow structures are formed during MOF synthesis by growing the framework around a sacrificial template, such as silica or polystyrene spheres, followed by template removal. For instance, Yang *et al.* synthesized hollow porous carbon (HPC) by pyrolyzing ZIF-8 grown on PS templates, resulting in a porous shell with high surface area that significantly enhances catalytic efficiency[113] [Figure 6A]. In contrast, Yu *et al.* adopted a post-processing strategy as shown in Figure 6B, constructing hollow ZIF-67 prismatic nanostructures through rapid ion exchange using $Co(CH_3COO)_2(OH)_3$ nanoprisms as sacrificial templates[114]. Subsequent sulfidation transformed these into hollow $CoS_2$ particles that retained the prismatic morphology. The formation of the hollow interior is driven by the outward diffusion of $Co^{2+}$ ions from the precursor nanoprisms and the inward migration of organic ligands, leading to the oriented growth of ZIF-67 polyhedra on the template surface and ultimately yielding well-defined hollow structures[115].

Subtle variations in reaction conditions can significantly influence the final morphology and composition of products. Yang *et al.* highlighted the role of solvent mediation in shaping bimetallic ZIF structures[116], demonstrating that hollow Co-ZIF phases can be transformed from ZIF-67 seeds in methanol through $Co^{2+}$ assistance (Figure 6C upper). This strategy was extended to the synthesis of hollow Zn/Co ZIF. The core shell ZIF-67@ZIF-8 intermediate further experienced $Co^{2+}$-driven structural transformation in methanol. The gradual variation in Zn concentration suggests the reconstruction of the core shell architecture, finally producing hollow rhombohedral dodecahedra with a Co rich ZIF-67 core wrapped by a Zn containing ZIF-8 shell (Figure 6C below).

Hollow LDH nanostructures derived from MOFs have also emerged as promising materials for catalysis and energy storage. Their work revealed that the kinetics of ZIF-8 etching and LDH nucleation must be carefully balanced to achieve well-defined hollow structures, emphasizing the critical role of reaction rate matching in structural evolution.

The post-processing approach involves the formation of hollow structures through the modification of pre-synthesized MOFs. As an effective strategy,

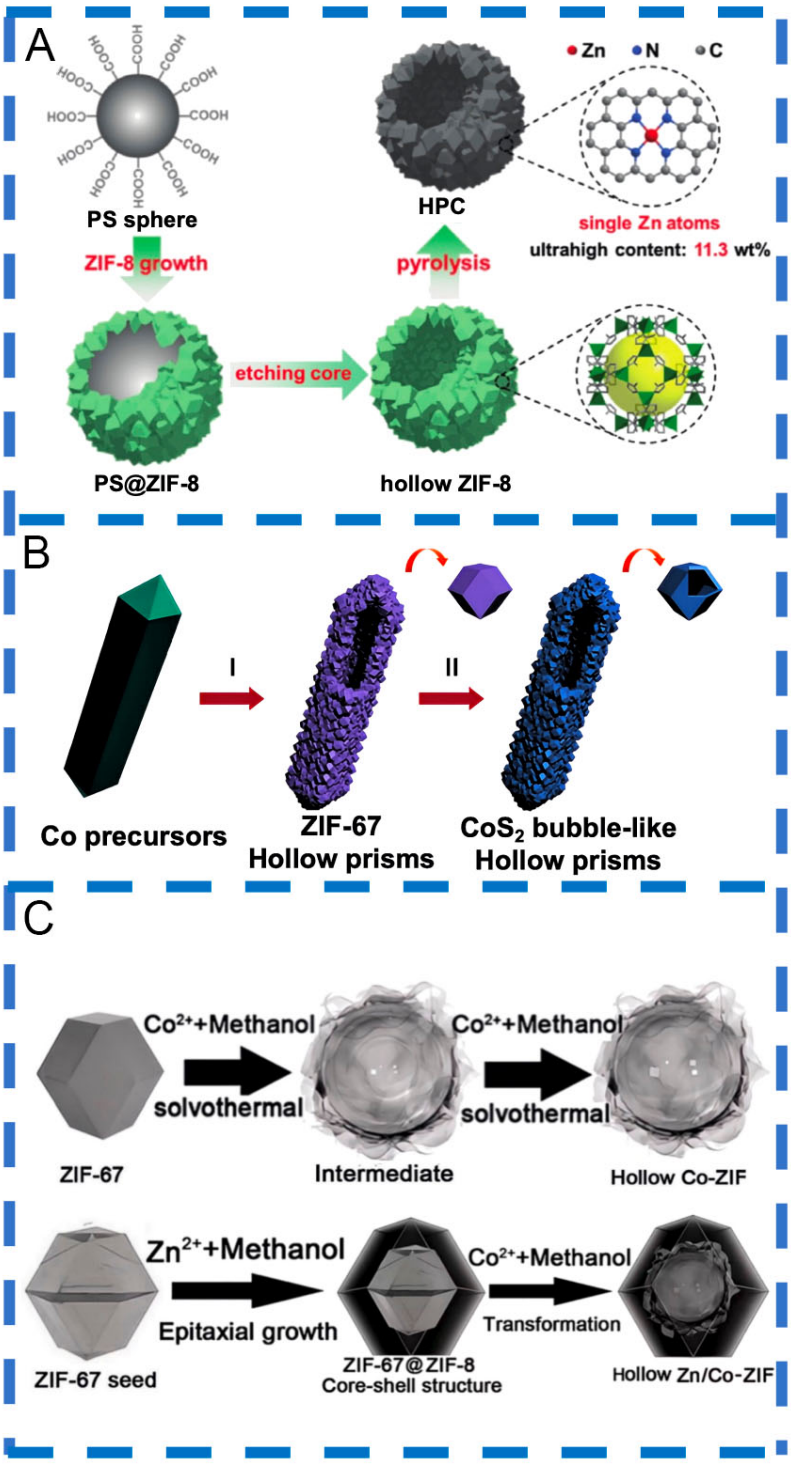


**Figure 6.** Schematic illustration showing (A) the preparation process of the HPC; This figure is adapted from Ref.[113]. Copyright@2019, Wiley-VCH; (B) Formation of $CoS_2$ nanobubble hollow prisms; This figure is adapted from Ref.[114]. Copyright@2016, Wiley-VCH; (C) Structural evolution of ZIF-67. This figure is adapted from Ref.[116]. Copyright@2015, Wiley-VCH. PS: Polystyrene; ZIF: zeolitic imidazolate framework; HPC: hollow porous carbon.

etching eliminates the need for template removal and offers distinct advantages over hard-templating methods, which often rely on particle agglomeration[117]. In contrast, etching can be applied to single-crystalline MOFs, enabling precise control over cavity dimensions and shell thickness by modulating the etching extent. To achieve well-defined hollow structures via chemical etching, the integrity of the MOF shell must be maintained throughout the process[118]. TA has been widely

employed for this purpose, owing to its strong surface adhesion and metal-coordination capabilities, as noted in Section **Exchange of metal ions**[119]. During etching, TA forms a protective layer on the MOF surface, preventing structural collapse, while the released protons diffuse inward to selectively remove the core. The molecular size of the etchant is critical: appropriately sized agents ensure uniform surface coverage and controlled etching, whereas mismatched sizes may lead to irregular pore formation or framework degradation[120]. A low defect concentration generally increases the population of accessible metal centers without significantly disrupting the continuous framework. Missing-linker defects remove steric constraints around adjacent metal nodes and expose open coordination positions for the adsorption of $H_2O$, $OH^-$, $H^+$, oxygen-containing intermediates, electrolyte ions, or sensing targets[121]. These coordinatively unsaturated sites may also possess altered electron density because cleavage of a metal-ligand bond changes the local ligand field and metal oxidation environment. Consequently, sparse defects can increase the number of active sites and improve the intrinsic reactivity of neighboring metal centers. At an intermediate defect concentration, isolated vacancies begin to form interconnected defective regions and hierarchical pores[122]. This defect level is often electrochemically favorable because it combines a high density of unsaturated metal sites with shortened ion-diffusion pathways and improved electrolyte penetration. Moderate etching can also promote charge redistribution, facilitate the formation of mixed-valence metal centers, and provide preferential nucleation sites for hydroxides, phosphides, sulfides, or metallic nanoparticles. Controlled formic acid modification changes the distribution and accessibility of unsaturated metal sites without completely destroying the crystalline phase. Formic acid, for instance, can modify MOF surfaces without altering their crystalline phase. It modulates the distribution and accessibility of unsaturated metal sites, thereby enhancing porosity, specific surface area, and charge transfer efficiency, which collectively improve electrochemical and catalytic performance[123].

Excessive etching may cause vacancy coalescence, extensive metal-node dissolution, linker loss, pore-wall thinning, and partial amorphization or collapse of the framework. Although severe etching can produce a high geometric surface area, it may interrupt electron-transfer pathways, decrease mechanical stability, promote active-metal leaching, and generate poorly connected or inaccessible pores. An excessively high density of unsaturated sites may also bind reaction intermediates too strongly, hinder product desorption, or accelerate undesired electrolyte decomposition. Therefore, electrochemical activity is expected to exhibit an optimum with increasing defect concentration: activity initially increases because more accessible and electronically modified sites are generated, reaches a maximum when active-site density and transport efficiency are balanced, and subsequently decreases when structural and electronic continuity are substantially damaged. This non-monotonic relationship should be considered when comparing samples prepared using different etchant concentrations, reaction times, temperatures, or solvent compositions.

In addition to acid etching, metal ion etching was discussed in Section **Exchange of metal ions**. Another notable method is oxidative linker cleavage within single-crystalline MOFs, introduced by Xia *et al.*[124]. The performance change can be more directly associated with etching-induced missing-linker or missing-node defects, coordinatively unsaturated metal sites, enlarged pores, and shortened diffusion pathways with no substantial phase transformation occurring.

Undoubtedly, while a variety of heterostructures can be derived from MOFs through etching, core-shell and hollow configurations remain among the most representative and widely studied[125]. These two architectures offer distinct advantages: both significantly enhance the accessibility and exposure of active sites. Furthermore, the combination of intrinsic microporosity from the MOF framework and newly created mesoporosity from etching synergistically facilitates efficient mass transport within the structure[126]. This hierarchical porosity markedly improves ion diffusion and charge transfer, contributing substantially to enhanced electrochemical performance.

To establish a meaningful defect-activity relationship, the defect descriptors should be correlated with both geometric and intrinsic electrochemical metrics. Electrochemically active surface area, dou-

ble-layer capacitance, redox charge, and probe adsorption can estimate the number of accessible sites[127], whereas turnover frequency or current normalized by the quantified active-site density can evaluate intrinsic activity per site. Electrochemical impedance spectroscopy[128] can determine whether increasing defect concentration improves or impairs charge-transfer resistance. Combining these measurements with density functional theory calculations of charge density, density of states, adsorption free energies, and ion-migration barriers can distinguish whether the activity enhancement originates primarily from an increased number of active sites[129], altered electronic structure, accelerated mass transport, or their cooperative effects. Accordingly, future studies should report etching parameters together with quantitative defect descriptors and site-normalized electrochemical performance, rather than relying solely on morphology, BET surface area, or geometric current density.

The beneficial effects of etching-induced defects must be balanced against the progressive loss of framework stability. Defect formation involves the cleavage of metal-linker coordination bonds that originally maintain the connectivity and mechanical integrity of the MOF lattice. At a relatively low defect concentration, isolated missing-linker defects and coordinatively unsaturated metal sites can be generated while the overall crystalline network remains intact[130]. These defects increase the accessibility and chemical reactivity of metal centers without substantially disrupting long-range connectivity. As the etching extent increases, neighboring vacancies may merge into defect clusters, mesopores, and internal cavities, improving mass transport and exposing a larger fraction of the framework. However, continued removal of linkers or metal nodes progressively reduces the number of load-bearing coordination bonds, weakens the pore walls and shell, and increases the susceptibility of the material to hydrolysis, dissolution, mechanical deformation, and electrochemical reconstruction.

Accordingly, optimal etching should be defined as the condition that maximizes the density and accessibility of chemically active defects while maintaining sufficient metal-linker connectivity, shell integrity, electrical continuity, and resistance to leaching. Future studies should therefore report activity and stability as coupled optimization targets rather than treating defect creation as an exclusively beneficial process.

## THE APPLICATION OF ETCHING MOFS

### Electrolysis of water

Electrocatalytic water splitting is a promising method for converting electrical energy into chemical energy stored in hydrogen, offering a sustainable pathway for hydrogen production. During this process, the hydrogen evolution reaction (HER) takes place at the cathode, involving a two-electron transfer process that leads to the formation of H-H bonds[131]. Simultaneously, the oxygen evolution reaction (OER) occurs at the anode, comprising a complex multi-step mechanism involving O-H bond cleavage and O-O bond formation through proton-coupled electron transfers[132]. The intricate nature of OER results in inherently slow reaction kinetics, necessitating high overpotentials that limit the overall efficiency of water splitting and reduce the rate of oxygen generation. As a result, the OER half-reaction is widely regarded as the bottleneck in electrocatalytic water splitting[133].

Phosphides exhibit remarkable properties such as high electrical conductivity, favorable electronic structure, and strong corrosion resistance, making them highly suitable for electrocatalytic applications. Specifically, cobalt phosphide (CoP) demonstrates high activity towards OER, attributed to the strong adsorption of oxygen intermediates on positively charged cobalt sites and facilitated $O_2$desorption by negatively charged phosphorus[134]. He *et al.* developed carbon-doped metal phosphide nanocubes derived from ZIF-67 to enhance OER performance[135]. Initially, ZIF-67 nanocubes were synthesized via a surface-mediated method, then transformed into Ni-Co LDH through etching, and finally converted into Ni-Co mixed metal phosphide (NiCoP and NiCoP/C) through phosphorylation using $NaH_2PO_2$ [Figure 7A]. Among these, the hollow NiCoP/C nanoboxes achieved an overpotential of 330 mV at 10 mA $cm^{-2}$ [Figure 7B], leveraging both the inherited high surface area and improved electrical conductivity from the MOF-derived hollow structure. These findings underscore the importance of morphological control in optimizing nanomaterial performance.

The newly formed inorganic phase commonly deter-

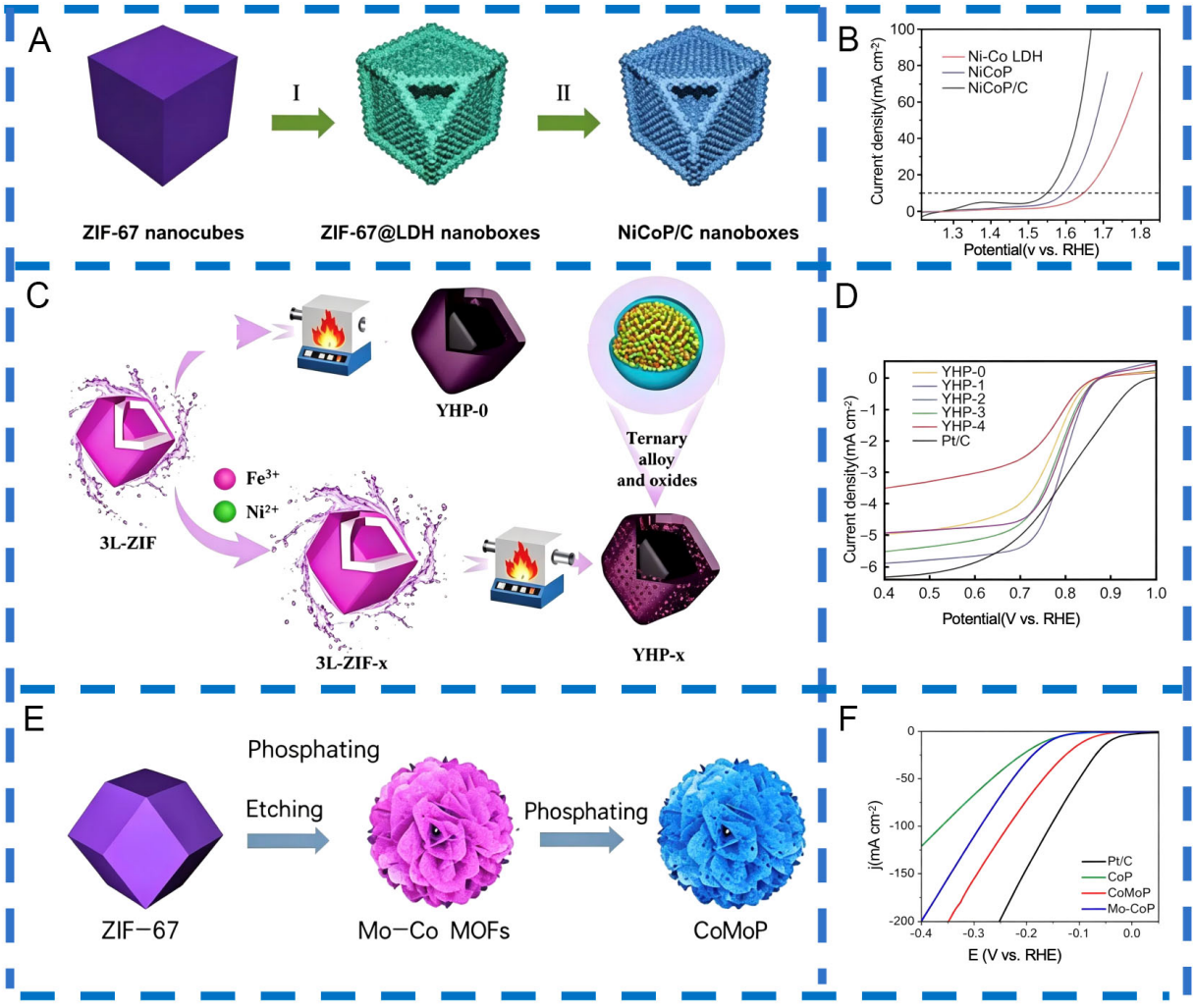


**Figure 7.** (A) Schematic illustration of the formation of NiCoP/C nano-boxes; (B) Polarization curves of Ni-Co LDH, NiCoP and NiCoP/C nano-boxes; (A and B) are reprinted with permission from Ref.[135]. Copyright@2017, Wiley-VCH; (C) Schematic illustration of synthetic procedure for YHP-x; (D) LSV curves toward OER; (C and D) are reprinted with permission from Ref.[137]. Copyright@2023, Springer Nature; (E) Schematic illustration of the CoMoP synthesis; (F) HER Polarization curves; (E and F) are reprinted with permission from Ref.[139]. Copyright@2022. Licensed under CC BY 4.0. ZIF: Zeolitic imidazolate framework; LDH: layered double hydroxide; RHE: reversible hydrogen electrode; YHP: yolk-shell hollow polyhedra; MOF: metal-organic framework; LSV: linear sweep voltammetry; OER: oxygen evolution reaction; HER: hydrogen evolution reaction.

mines the intrinsic catalytic sites and principal redox chemistry, whereas etching controls the precursor morphology, elemental distribution, defect density, and accessibility of the final phase. The phosphide phase provides substantially higher electrical conductivity and different adsorption properties for oxygen-containing intermediates compared with the hydroxide precursor, while the carbon component further improves electron transport and suppresses particle aggregation. The hollow architecture produced through etching reduces ion- and gas--transport distances. Therefore, the final OER performance results from the cooperation of the NiCoP active phase, the conductive carbon matrix, and the etching-derived hollow morphology.

Beyond conventional acid etching, we also developed an electrochemical Lewis acid co-etching and electrochemical adsorption doping method to incorporate larger-radius Hf ions into Co-MOF[136]. This approach introduced beneficial defects and markedly enhanced OER kinetics, as evidenced by a significant reduction in the Tafel slope. This strategy of doping high-valence metals offers a novel pathway for designing high-performance electrocatalysts. Given the challenging four-electron transfer processes in both OER and the oxygen reduction reaction (ORR), designing efficient and stable bifunc-

**Table 2. Quantitative comparison of representative etched MOF-derived electrocatalysts for water splitting**

| Catalyst | Precursor | Reaction | Electrolyte | $H_{10}$ (mV) | Tafel slope (mV $dec^{-1}$) | Stability | Ref. |
|---|---|---|---|---|---|---|---|
| NiCoP/C nanoboxes | ZIF-67 nanocubes | OER | 1.0 M KOH | 330 | 96 | - | [135] |
| Hf/XO-CoP-350 | Truncated ZIF-67 | OER | 1.0 M KOH | 292 | 90.8 | 25 h | [136] |
| (Fe,Hf)CoOOH/ $Co(OH)_2$ | Co-MOF | OER | 1.0 M KOH | 250 | 37.6 | - | [136] |
| YHP-2 | 3L-ZIF | OER | NR | 257 | - | - | [138] |
| YHP-1 | 3L-ZIF | ORR | NR | - | - | - | [138] |
| CoMoP nanosheets | ZIF-67 | OER | 1.0 M KOH | 273 | 54.9 | 3% current loss after 100 h | [140] |
| CoMoP nanosheets | ZIF-67 | HER | 1.0 M KOH | 89 | 69.7 | 6% current loss after 100 h | [140] |
| Hollow $CoS_2$-$MoS_2$ arrays | Co-MOF | HER | Alkaline electrolyte | 82 | - | > 24 h | [141] |
| Hollow $CoS_2$-$MoS_2$ arrays | Co-MOF | OER | Alkaline electrolyte | 266 | - | > 24 h | [142] |

ZIF: Zeolitic imidazolate framework; OER: oxygen evolution reaction; YHP: yolk-shell hollow polyhedra; ORR: oxygen reduction reaction; MOF: metal-organic framework; HER: hydrogen evolution reaction.

tional catalysts is crucial for overall water splitting and regenerative fuel cells. Using a triply layered ZIF precursor[137], we constructed yolk-shell hollow polyhedra (YHPs) embedded with ternary alloys and metal oxides through precisely controlled etching and pyrolysis [Figure 7C]. These YHP catalysts outperformed commercial benchmarks in both OER and ORR [Figure 7D], owing to the etching role of Lewis acid in forming yolk-shell configurations that provide abundant active sites and enhance mass and charge transfer.

As highlighted in previous sections, the development of bifunctional catalysts is critical for efficient electrocatalytic processes. While OER bifunctional catalysts have been widely explored, significant progress has also been made in designing HER/OER bifunctional catalysts for overall water splitting[138]. For instance, Wang *et al.* synthesized ultrathin CoMoP nanosheets through ion etching and phosphorylation of ZIF-67 [Figure 7E][139]. Treatment with ammonium molybdate induced both structural etching and partial substitution of $Co^{3+}$ by $Mo^{6+}$, resulting in a porous, folded Mo-Co MOF intermediate. Subsequent phosphorylation produced bimetallic phosphide nanosheets that exhibited exceptional activity and stability for both HER and HER [Figure 7F].

Compared to their pristine counterparts, etched MOFs demonstrate superior and tunable functional properties[140]. The quantitative comparison of representative etched MOF-derived electrocatalysts for water splitting is displayed in Table 2. Etching serves as a versatile and efficient strategy for tailoring MOF-derived materials, enabling the creation of well-defined pore systems and the introduction of heteroatoms without phase segregation[141]. The incorporation of suitable foreign metal species further modulates the electronic structure and enhances electrical conductivity, leading to improved electrocatalytic performance. Overall, the strategic optimization of both structure and composition is indispensable for advancing the efficacy of MOF-based electrocatalysts[142].

## Supercapacitors

Supercapacitors represent a class of energy storage devices operating through Faradaic electrochemical processes, renowned for their long cycle life, rapid charge-discharge capability, and operational safety[143]. The capacitance of their electrode materials originates from surface-mediated processes, including electrochemical adsorption/desorption of ions and reversible redox reactions at the electrode--electrolyte interface[144].

Etched MOFs and their derivatives have emerged as high-performance electrode materials in supercapacitors, primarily due to their elevated specific surface area, abundant active sites, and tailored porosity resulting from etching, which collectively contribute

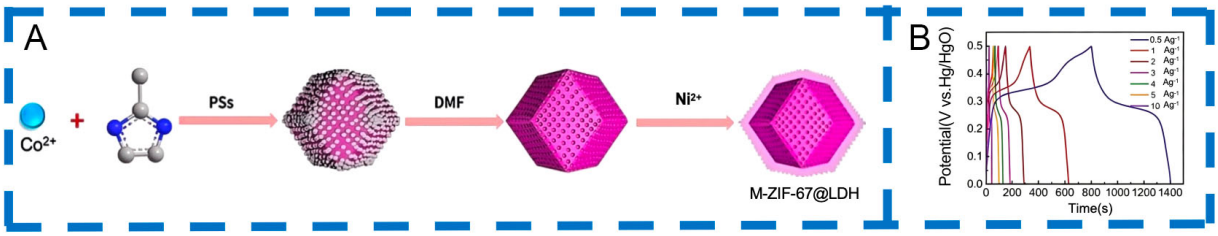


**Figure 8.** (A) The schematic diagram of the synthesis of M-ZIF-67@LDH4; (B) GCD curves of M-ZIF-67@LDH at current densities of 0.5-10 A $g^{-1}$; (A and B) are reprinted with permission from Ref.[151]. Copyright@2021, Wiley-VCH. ZIF: Zeolitic imidazolate framework; PS: polystyrene; DMF: N,N-dimethylformamide; GCD: galvanostatic charge-discharge; LDH: layered double hydroxide.

to high specific capacitance[145]. When MOFs are etched with metal ions, they can be transformed into ultrathin bimetallic hydroxide nanosheets with hollow architectures[146]. The combination of layered morphology and hollow features accelerates ion diffusion, enabling efficient Faradaic redox reactions even at high current densities and thereby enhancing rate capability. This approach offers a generalized strategy for designing high-performance LDH-based energy materials. The evolution from bulk particles to ultrathin nanosheets or open nanocages also affects Faradaic kinetics[147]. Thinner nanosheets reduce the distance required for electrolyte ions to reach redox-active metal centers and increase the proportion of edge and surface sites.

Hollow-structured nanomaterials have garnered significant research interest for their promising applications in energy storage due to their high surface area, efficient mass transport, and tunable porosity[148,149]. For instance, Tang *et al.* synthesized hollow nano-polyhedra using ZIF-67 as a template, systematically investigating the critical roles of shell precipitation and template etching in nanocage formation[150]. The resulting NiCo-LDH nanocages demonstrated excellent pseudocapacitive performance. In related work[151], our group designed core-shell structures using macro-microporous ZIF-67 (M-ZIF-67) grown on PS templates as the core and LDH as the shell through facile ion etching [Figure 8A]. The optimized material, M-ZIF-67@LDH4, delivered a specific capacitance of 597.6 F $g^{-1}$ at 0.5 A $g^{-1}$ and maintained 92% retention at 3 A $g^{-1}$ [Figure 8B], underscoring the synergistic enhancement from its hierarchical porosity and LDH integration.

The application of etched MOFs in supercapacitors has demonstrated considerable promise. By precisely tailoring the structure and properties of electrode materials, etching strategies have markedly improved key performance metrics including specific capacitance, rate capability, and cycling stability[152]. Nevertheless, challenges such as limited electrical conductivity, long-term operational stability, and scalable production costs must be addressed to facilitate their practical implementation in commercial supercapacitors. Future research should focus on advancing novel etching methodologies, designing multifunctional composite architectures, and elucidating underlying reaction mechanisms[153]. These efforts are expected to open new avenues for developing high-performance, economically viable supercapacitors.

## Battery

Rechargeable batteries including lithium-ion, metal-air, and zinc-manganese systems are extensively utilized across numerous applications due to their high energy density and reversible operation[154]. Etching MOFs has emerged as an efficient strategy for synthesizing advanced electrode materials with superior energy storage performance[155]. The enhancements are primarily attributed to the following structural and functional advantages introduced by etching: (a) Hierarchically porous and hollow structures facilitate rapid ion and electrolyte transport, improving electrode-electrolyte contact; (b) Hollow architectures effectively accommodate volume changes during cycling, enhancing rate capability and long-term cyclability; (c) High specific surface area provides abundant electrochemically active sites, resulting in increased specific capacity.

Etched MOFs have been widely employed as electrodes in various battery systems. Here, we focus

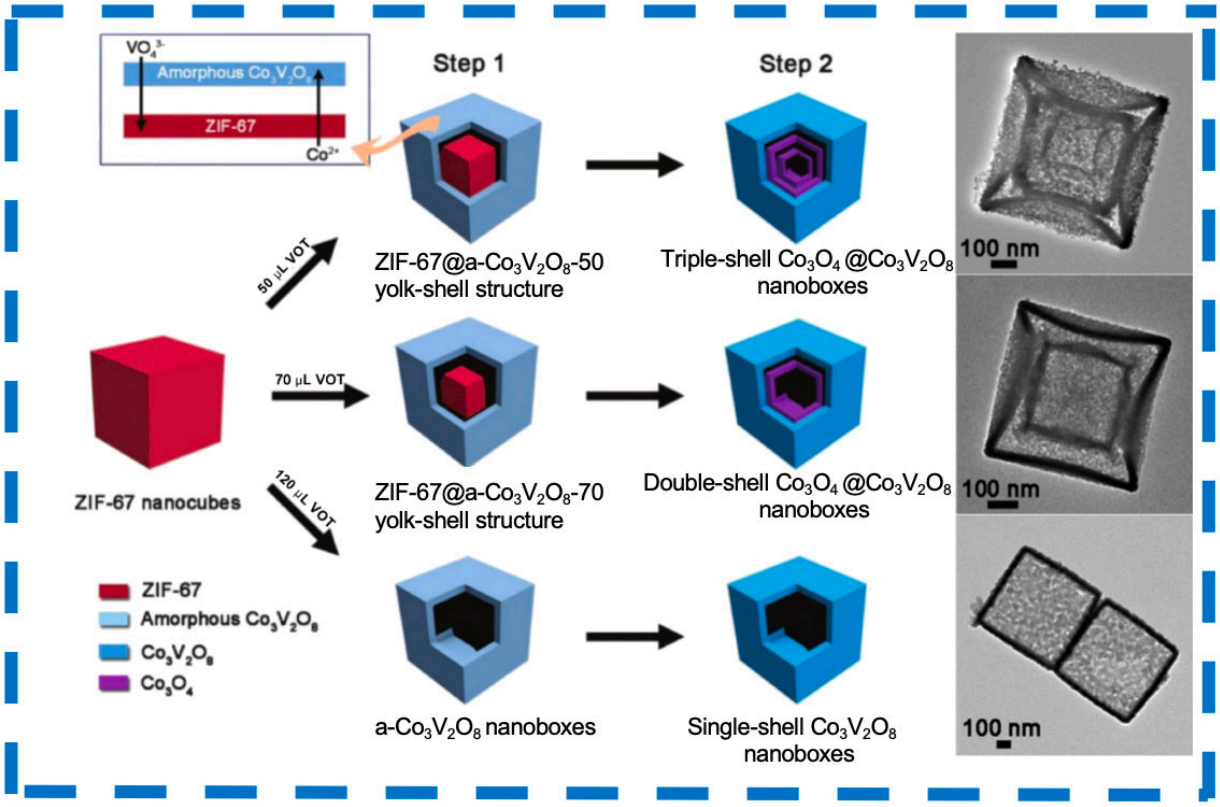


**Figure 9.** Schematic illustration of the formation of different shelled nanostructures; This figure is adapted from Ref.[156]. Copyright@2018, Wiley-VCH. ZIF: Zeolitic imidazolate framework.

on lithium-based batteries, which represent a leading direction in energy storage research. In 2018, Lu *et al.* fabricated multi-shelled nanostructures with tunable shell numbers and evaluated their performance as anodes for lithium-ion batteries[156]. As illustrated in Figure 9, simply by varying the amount of vanadium oxytriisopropoxide (VOT) during ion exchange with ZIF-67 nanocubes followed by calcination in air, they obtained nanoboxes with single, double, and triple shells. Electrochemical analysis revealed that the triple-shelled nanostructure delivered the most exceptional performance, a result directly attributable to its uniquely engineered architecture.

The confinement of active nanomaterials within porous carbon matrices has proven to be an effective strategy for enhancing the electrochemical properties of lithium-ion batteries[157,158]. While carbon materials derived from MOFs hold great promise as electrodes, their inherently small pore sizes often limit accessibility to active sites during cycling[159]. To address this limitation, the same research group developed hollow nanostructures designated as H-$Co_3O_4$@MCNBs two years later[160]. These consist of hollow $Co_3O_4$ nanoparticles encapsulated within mesoporous carbon nanoboxes, fabricated through a combination of etching and a carefully controlled two-step thermal treatment. This distinctive structure and composition endow the H-$Co_3O_4$@MCNBs with remarkable lithium storage capabilities as an anode material, including high discharge/charge capacities and excellent Coulombic efficiency.

Lithium-sulfur (Li-S) batteries have attracted considerable attention for their high theoretical capacity and energy density[161]. However, practical implementation is hindered by the insulating nature of sulfur, the shuttle effect of polysulfide intermediates, and substantial volume changes during cycling[162]. Hollow frameworks offer a promising solution to accommodate volume expansion and enhance reaction kinetics[163]. Wang *et al.* constructed hollow ZnSe-CoSe heterostructures with tunable cavity sizes through etching of ZIF-8@ZIF-67 precursors followed by gas-phase selenization[164]. Furthermore, by integrating 45@ZnSe-CoSe with conductive MXene

nanosheets, a high sulfur-loading cathode was achieved. The resulting battery exhibited exceptional performance, highlighting the effectiveness of this hollow heterostructure design in mitigating the challenges of Li-S batteries[165].

As evidenced by recent advances, the application of etched MOFs represents a highly promising direction in battery research. Through precise structural and compositional regulation, etching techniques significantly enhance the electrochemical performance of MOF-based electrodes[166]. By selectively removing parts of the framework, etching creates porous or hollow architectures that increase specific surface area and porosity, thereby promoting ion diffusion and improving active site utilization[167].

Moreover, etched MOF structures exhibit improved mechanical stability, effectively mitigating volume changes during ion insertion and extraction. In the context of solid-state batteries, the porous networks formed via etching offer additional ion transport pathways, contributing to higher ionic conductivity of the electrolyte[168,169]. These advantages collectively position etched MOFs and their derivatives as highly competitive materials for next-generation energy storage systems.

### Electrochemical sensing

In addition to the above applications, MOFs are also used in electrochemical sensing and have demonstrated great potential. By regulating the structures and components, the sensitivity, selectivity and stability of the sensors based on etched MOFs and MOF derivatives have been significantly enhanced[170,171]. Etching facilitates the creation of rich pores to facilitate the diffusion of materials and exposure of plenty of surface-active sites, enabling high sensing performance.

In the work of Zeng *et al.*, they obtained hierarchical hollow MIL-101 cages simply via acid etching and employed them in the electrochemical sensor[172]. Attributed to the huge specific surface area and adsorptive property, the hollow MIL-101 denoted high electrocatalytic activity and fantabulous voltammetric response towards the nitrofurazone oxidation. Apparently, compared with solid crystals, the design of hollow structures contributes to extraordinary electrocatalytic activity.

In summary, etching is a useful tool for tailoring the structure, composition, electronics, and physiochemistry of MOFs, and these beneficial changes help improve the performance of the target application. Future research directions include the development of novel etching techniques, the preparation of multifunctional composite materials, and in-depth studies on the mechanism of reaction, which should provide new ideas and methods for the design of high-performance electrochemical sensors.

## CONCLUSIONS AND PERSPECTIVE

In this review, we have summarized key strategies for etching MOFs, highlighted the distinctive nanostructures obtained through these processes, and discussed the roles of etched MOFs across various electrochemical applications. Etching significantly enhances mass transport, exposes abundant active sites, and provides void space to accommodate volume changes during energy conversion and storage, collectively improving the overall performance of MOF-based electrodes.

It is important to note that etching mechanisms can vary considerably across different MOFs, even when using the same etchant. Therefore, combined experimental and theoretical investigations are essential to elucidate these mechanisms, identify key influencing factors, and optimize etching conditions. For instance, while monocarboxylic acids primarily disrupt UiO-type frameworks through acid-induced coordination cleavage, in ZIFs, proton attack plays a dominant role. Excessive etching must be avoided as it can cause structural collapse and loss of porosity. Parameters such as etchant concentration, temperature, pH, and duration must be carefully controlled to achieve desired pore structures, exposed facets, morphologies, and compositions. Moving forward, the cost efficiency and environmental impact of etching agents and protocols should also be prioritized.

Although etching provides an effective route for regulating MOF porosity, defects, and morphology, its environmental impact and scale-up feasibility require more careful consideration. High-temperature post-treatments, including carbonization, phosphidation, sulfurization, and thermal phase conversion, can substantially increase energy consumption, particularly when prolonged heating under an inert atmosphere is required. Multistep washing, solvent

**Table 3. Summary of representative etched MOFs, etching routes, derived structures and electrochemical applications**

| Precursor MOF | Etching classification | Etchant/Template | Key synthetic conditions | Final microstructure | Electro-chemical application | Ref. |
|---|---|---|---|---|---|---|
| ZIF-8 | Hard template etching | ZnO nanorods, KOH | 70 °C, 24 h, calcination | N-doped hollow carbon microtubules | Li-S battery cathode | [41] |
| ZIF-67 | Hard template etching | ZIF-67 (sacrificial template), CTAB | Room temperature, magnetic stirring | Hollow polyhedron | Li-$O_2$ battery cathode catalyst | [43] |
| ZIF-67 | Hard template etching | Cubic ZIF-67, Co-Fe PBA | Annealing treatment | Hollow CoFe@C nanoboxes | Electrocatalytic water splitting | [49] |
| ZIF-8 | Hard template etching | Carboxyl-terminated PS | Solvothermal reaction | Hollow ZIF-8 microspheres | Supercapacitor | [52] |
| ZIF-8 | Soft template etching | SDS anionic micelles | Aqueous solution, room temperature | Hollow ZIF-8 nanospheres | OER electrocatalysis | [61] |
| ZIF-67 | Soft template etching | $C_n$TAB cationic vesicles | Aqueous solution, DMF/MeOH washing | Uniform hollow ZIF-67 particles | Overall water splitting | [63] |
| ZIF-67 | Metal ion & acid synergistic etching | TA | Room temperature, variable etching time | Hollow Co@NCN polyhedra | OER/HER bifunctional catalysis | [71] |
| MIL-101(Cr) | Metal ion / Acid etching | Acetic acid | Stepwise crystal growth + etching | Single/double/triple-shell hollow MIL-101(Cr) | Electrocatalysis | [74] |
| v-1 | Acid etching | Phosphoric acid | Variable acid concentration & etching time | Defect-rich porous Cu-based MOF | Supercapacitor | [75] |
| ZIF-67 | Acid etching | Cyanuric acid (CA) | Selective facet passivation | Hollow nanoframes | Electrocatalysis | [76] |
| ZIF-67 | Metal ion etching | $Co^{2+}$, $Ni^{2+}$ | Hydrothermal reaction | Bimetallic NiCo-LDH hollow polyhedra | Supercapacitor | [81] |
| Co-ZIF-L | Metal ion etching | $Co^{2+}$, $Ni^{2+}$ | DMF-ethanol system, 70 °C | Tunable CoNi-LDH | Electrocatalytic water splitting | [83] |
| ZIF-67 | Metal ion etching | $Ni^{2+}$, $Fe^{2+}$ | Adjustable ethanol/water ratio | Single/double-shell Ni-Fe LDH nanocages | Supercapacitor | [87] |
| ZIF-67 | Mixed acid & metal ion etching | $Ni^{2+}$, Boric acid ($H_3BO_3$) | One-pot reaction | Hollow carbon polyhedra | Electrocatalysis | [91] |
| Cu-MOF-74 | Ligand (alkaline) etching | KOH, $Na_2S$ | 100 °C, hydrothermal treatment | Hollow copper sulfide | Supercapacitor | [94] |
| Co-Co PBA | Ligand (alkaline) etching | Ammonia solution ($NH_3{\cdot}H_2O$) | Water-ethanol mixed solvent | Hollow Cu-$CoSe_2$ nanoframes | OER electrocatalysis | [95] |
| MIL-88A | Ligand dry etching | Thiourea | 650 °C, $N_2$ atmosphere | $Fe_7S_8$/C composites | Electrocatalysis | [96] |
| NiCo-PBA | Ammonia-assisted ligand etching | $NH_3{\cdot}H_2O$, $Cu^{2+}$, $Se^{2+}$ | Room temperature reaction | Dodecagonal N-doped carbon nanosheets | Water splitting catalysis | [97] |
| ZIF-8 | Hard template + core-shell construction | CdS nanoparticles, PVP | Two-step growth | CdS@ZIF-8 core-shell structure | Electrocatalysis | [108] |
| UiO-66-$NH_2$ | Epitaxial growth + mild etching | $Fe_3O_4$ nanoparticles | Layer-by-layer immersion & magnetic separation | $Fe_3O_4$@UiO-66-$NH_2$ core-shell | Electrochemical sensing | [110] |
| MIL-101 | Water etching | Mesoporous silica ($mSiO_2$), deionized water | Room temperature water treatment | Yolk-shell MOF@$mSiO_2$ | Catalysis & sensing | [111] |
| ZIF-67 | Metal ion etching + phosphating | $Ni(NO_3)_2$ $NaH_2PO_2$ | High-temperature phosphating | Hollow NiCoP/C nanoboxes | OER catalysis | [135] |
| ZIF-67 | Metal ion etching | $Co^{2+}$, $Ni^{2+}$, PNT substrate | Solvothermal reaction | PNT@NiCo-LDH nanocages | Hybrid supercapacitor | [149] |

| | | | | | | |
|---|---|---|---|---|---|---|
| MIL-101 | Acid etching | Organic acid | Controlled acid corrosion | Hierarchical hollow MIL-101 cages | Electrochemical sensing | [172] |

MOF: Metal-organic framework; ZIF: zeolitic imidazolate framework; CTAB: cetyltrimethylammonium bromide; DMF: N,N-dimethylformamide; TA: tannic acid; PS: polystyrene; HKUST: Hong Kong University of Science and Technology; NiCo-PBA: PVP: polyvinylpyrrolidone; PNT: Polypyrrole Nanotube; LDH: layered double hydroxide; MIL: Materials of the Institute Lavoisier; OER: oxygen evolution reaction.

exchange, and repeated growth-etching cycles also increase water and solvent usage and reduce overall material yield. By comparison, conventional acid- or base-assisted wet etching is generally conducted under mild temperatures using inexpensive and readily available reagents, making it economically attractive for large-scale production. However, its apparent cost advantage may be partly offset by equipment corrosion, neutralization requirements, metal-containing wastewater, salt generation, and the consumption of large volumes of washing water. Strong oxidants, organic solvents, and fluorine-containing etchants may create additional safety and environmental burdens. Future scale-up should therefore prioritize dilute and recyclable etchants, aqueous or low-toxicity solvent systems, closed-loop reagent recovery, continuous-flow processing, reduced washing steps, and low-temperature phase conversion. Evaluating reagent utilization, product yield, energy input, wastewater generation, and recyclability through techno-economic analysis and life-cycle assessment will be essential for determining whether an etching strategy remains advantageous beyond laboratory-scale synthesis.

Furthermore, regarding the existing doubt of high-cost organic ligand consumption for pristine MOF followed by etching-induced partial framework loss: from an industrial and resource circulation perspective, precision-controlled etching is an economically favorable modification path for advanced electrochemistry materials. First, hollow/graded porous architecture obtained by etching drastically improves active site exposure and electrolyte penetration, lifting unit-mass electrochemical capacity to compensate precursor ligand cost; second, etching can convert cheap commercially available bulk MOF powder into high-value hierarchical electrode/catalyst that cannot be directly synthesized with low-cost raw materials via one-pot route; third, spent etched MOF derivatives after electrochemical failure can be recollected and re-etched for secondary structure reconstruction, realizing cyclic utilization of expensive metal and organic ligand resources and lowering overall material lifecycle cost. This practical economic advantage further highlights the necessity and potential value of continuous research on precise etching of MOFs. To provide a clear overview of the three aspects including etching methods, post-etching material structures, and applications, we have listed the references on etched MOFs discussed in this review in Table 3.

In terms of applications, we have focused on electrocatalytic water splitting, supercapacitors, batteries, and sensors, though the potential of etched MOFs extends well beyond these areas. Long-term stability remains a critical challenge for practical deployment, as etching may compromise mechanical or chemical robustness. Balancing activity with stability through compositional tuning or integration with stable matrices is often necessary. To harness etched MOFs in high-performance devices, scenario-specific design and precise control over etching processes are imperative.

In summary, etching serves as a powerful tool to tailor the structure, composition, and properties of MOFs for enhanced electrochemical functionality. We hope this review offers a comprehensive overview of the current advances and future directions in etched MOFs, and inspires further innovative research in this rapidly evolving field.

## DECLARATIONS

### Authors' contributions

Writing - original draft preparation: Wang, S.
Data curation: Wang, S.
Visualization: Wang, S.; Li, S.
Data curation: Fan, J.
Methodology: Li, S.
Conceptualization: Shakouri, M.; Zhu, R.
Language polishing: Shakouri, M.
Supervision: Zhu, R.
Writing- reviewing and editing: Zhu, R.
Funding acquisition: Zhu, R.

### Availability of data and materials

Not applicable.

## AI and AI-assisted tools statement

The pictures of the hard template strategy (lower left), metal ion etching and exchange of ligands of Figure 1 were generated using the Doubao artificial intelligence system (Version 2026.07, released on 2026-07-16). The four schematic illustrations in the graphical abstract - water electrolysis, electrochemical sensing, battery, and supercapacitor - were generated using OpenAI's ChatGPT Images tool, powered by the GPT-Image-1.5 model (version 1.5 released on 2025-12-16). The tool did not influence the study design, data collection, analysis, interpretation, or the scientific content of the work. All authors take full responsibility for the accuracy, integrity, and final content of the manuscript.

## Financial support and sponsorship

This work was supported by the Natural Science Foundation of Jiangsu Province (BK20230069).

## Conflicts of interest

All authors declared that there are no conflicts of interest.

## Ethical approval and consent to participate

Not applicable.

## Consent for publication

Not applicable.



## REFERENCES

1. Chi, J.; Gu, S.; Shi, R.; et al. Extending PANI molecular chains into pores of hierarchical MIL-101 as flexible electrodes for supercapacitor applications. *Chem. Eng. J.* **2025**, *510*, 161764. DOI
2. Su, Y.; Shi, Y.; Jin, L.; et al. Unlocking the potential of MOFs for waste plastic resource utilization and microplastic pollution control. *Sustainable. Engineering. Novit.* **2026**, *2*, 4. DOI
3. Zhang, X.; Tang, Z.; Xu, H.; et al. Surface engineering of a MOF-on-MOF heterostructure via selenium oxide embedding for efficient seawater oxygen evolution. *Appl. Surf. Sci.* **2026**, *727*, 165837. DOI
4. Zhang, W.; Jiang, X.; Zhao, Y.; et al. Hollow carbon nanobubbles: monocrystalline MOF nanobubbles and their pyrolysis. *Chem. Sci.* **2017**, *8*, 3538-46. DOI PubMed PMC
5. Feng, J.; Liu, L.; Meng, Q. Enhanced electrochemical and capacitive deionization performance of metal organic framework/holey graphene composite electrodes. *J. Colloid. Interface. Sci.* **2021**, *582*, 447-58. DOI
6. Fu, R.; Wang, L.; Yang, X.; et al. Defects-Engineered Metal-Organic Frameworks for Supercapacitor Platform. *Sustainable. Engineering. Novit.* **2025**, *1*, 2. DOI
7. Zhang, Y.; Lan, J.; Xu, Y.; et al. Ultrafine PtCo alloy by pyrolysis etching-confined pyrolysis for enhanced hydrogen evolution. *J. Colloid. Interface. Sci.* **2024**, *660*, 997-1009. DOI
8. Abdi, M. R.; Sarlak, N.; Pourfalah, Z. HKUST-1@etched halloysite nanotube composites for enhanced cryogenic hydrogen adsorption. *Mater. Today. Commun.* **2026**, *51*, 114647. DOI
9. Acharya, J.; Ojha, G. P.; Kim, B.; Pant, B.; Park, M. Modish designation of hollow-tubular rGO-$NiMoO_4$@Ni-Co-S hybrid core-shell electrodes with multichannel superconductive pathways for high-performance asymmetric supercapacitors. *ACS. Appl. Mater. Interfaces.* **2021**, *13*, 17487-500. DOI PubMed
10. Aftab, A.; Ahmad, F.; Tunio, S. R.; Raza, N.; Salem, M. E.; Chaudhary, A. A. A critical review on electrochemical behavior of MOF in supercapacitor. *J. Organomet. Chem.* **2025**, *1042*, 123866. DOI
11. Gao, Y.; Ye, C.; Wang, R.; Li, W.; Pang, H. Hybrid and flow-electrode capacitive deionization: materials design, multispecies removal, and smart regulation. *Sustainable. Engineering. Novit.* **2025**, *1*, 7. DOI
12. Ahmed, A.; Hodgson, N.; Barrow, M.; et al. Macroporous metal-organic framework microparticles with improved liquid phase separation. *J. Mater. Chem. A.* **2014**, *2*, 9085-90. DOI
13. Yoon, J.; Shin, M.; Lim, J.; Lee, J.; Choi, J. Recent advances in MXene nanocomposite-based biosensors. *Biosensors.* **2020**, *10*, 185. DOI PubMed PMC
14. Alekseevskiy, P. V.; Timofeeva, M.; Bachinin, S.; et al. Non-thermal plasma etching of MOF thin films in high optical quality for interference sensing. *Opt. Mater.* **2024**, *154*, 115666. DOI
15. Sun, S.; Zhang, Y.; Wang, M.; et al. Design and fabrication of metal-organic framework UiO-66 membranes for advanced separation. *Sustainable. Engineering. Novit.* **2026**, *2*, 3. DOI
16. Baby, N.; Thangarasu, S.; Murugan, N.; Kim, Y. A.; Oh, T. Emerging SrFe-MOF/Fe-BTC hybrids via post-synthetic induced $Fe^{3+}$ metal node exchange and nucleation for durable bifunctional electrocatalysis. *Chem. Eng. J.* **2026**, *528*, 172235. DOI
17. Ban, Q.; Li, L.; Liu, H.; et al. Polymerization-induced assembly-etching engineering to hollow Co@N-doped carbon microcages for superior electromagnetic wave absorption. *Carbon.* **2023**, *215*, 118506. DOI
18. Bao, S.; Li, J.; Guan, B.; Jia, M.; Terasaki, O.; Yu, J. A green selective water-etching approach to MOF@mesoporous $SiO_2$ yolk-shell nanoreactors with enhanced catalytic stabilities. *Matter.* **2020**, *3*, 498-508. DOI
19. Bindini, E.; Lüdtke, T.; Otaegui, D.; et al. Mind the gap! *Inorg. Chem. Front.* **2022**, *9*, 221-30. DOI

20. Liang, Z.; Xie, J.; Liu, Q.; et al. Recent progress of metal-organic frameworks and derivatives for high-performance aqueous zinc-based batteries. *Sustainable. Engineering. Novit.* **2026**, *2*, 2. DOI
21. Dong, J.; Zhang, X.; Dong, X.; et al. Coupled porosity and heterojunction engineering: MOF-derived porous $Co_3O_4$ embedded on $TiO_2$ nanotube arrays for water remediation. *Chemosphere.* **2021**, *274*, 129799. DOI
22. Chen, X.; Liu, H.; Wang, L.; Wang, B. Morphology engineering of metal-organic frameworks by facet-selective protection and etching. *Inorg. Chem.* **2024**, *63*, 15574-8. DOI
23. Chen, H.; Gu, Z.; Mirza, S.; Zhang, S.; Zhang, J. Hollow Cu-$TiO_2$/C nanospheres derived from a Ti precursor encapsulated MOF coating for efficient photocatalytic hydrogen evolution. *J. Mater. Chem. A.* **2018**, *6*, 7175-81. DOI
24. Li, S.; Gao, Y.; Li, N.; Ge, L.; Bu, X.; Feng, P. Transition metal-based bimetallic MOFs and MOF-derived catalysts for electrochemical oxygen evolution reaction. *Energy. Environ. Sci.* **2021**, *14*, 1897-927. DOI
25. Lv, S.; Zhao, N.; Liu, J.; Yang, F.; Li, C.; Wang, S. Newly constructed $NiCo_2O_4$ derived from ZIF-67 with dual mimic enzyme properties for colorimetric detection of biomolecules and metal ions. *ACS. Appl. Mater. Interfaces.* **2021**, *13*, 25044-52. DOI
26. Tang, Z.; Wei, A. Fabrication of anisotropic metal nanostructures using innovations in template-assisted lithography. *ACS. Nano.* **2012**, *6*, 998-1003. DOI PubMed PMC
27. Drozhzhin, N. A.; Ponomareva, O. Y.; Vinogradov, I. I.; et al. Nickel (II) based metal-organic framework consolidated on nanofibers modified track-etched membrane for dye removal. *Eurasian. j. chem.* **2025**, *30*, 118-28. DOI
28. Chhetri, K.; Dahal, B.; Tiwari, A. P.; et al. Controlled selenium infiltration of cobalt phosphide nanostructure arrays from a two-dimensional cobalt metal-organic framework: a self-supported electrode for flexible quasi-solid-state asymmetric supercapacitors. *ACS. Appl. Energy. Mater.* **2021**, *4*, 404-15. DOI
29. Chen, L.; Liu, Y.; Su, Y.; Zhu, W.; Du, G.; Pang, H. Research progress in metal-organic frameworks and their derivatives in electrochemistry. *Sci. China. Chem.* **2025**, *68*, 1287-316. DOI
30. He, N.; Zou, Y.; Chen, C.; et al. Constructing ordered and tunable extrinsic porosity in covalent organic frameworks via water-mediated soft-template strategy. *Nat. Commun.* **2024**, *15*, 3896. DOI PubMed PMC
31. Qin, L.; Xiao, Z.; Zhai, S.; et al. Defect-rich N-doped porous carbon derived from alginate by $HNO_3$ etching combined with a hard template method for high-performance supercapacitors. *Mater. Chem. Phys.* **2021**, *260*, 124121. DOI
32. He, Y.; Fang, J.; Zhang, W.; et al. High-efficiency oxygen evolution electrocatalysis enabled by $Ar/O_2$ plasma-induced synergistic modifications in NiFe Prussian blue analogue systems. *RSC. Adv.* **2025**, *15*, 36206-12. DOI PubMed PMC
33. Qu, N.; Xu, G.; Liu, Y.; et al. Multi-scale design of metal-organic framework metamaterials for broad-band microwave absorption. *Adv. Funct. Mater.* **2025**, *35*, 2402923. DOI
34. Garg, R.; Alattar, B.; Sabouni, R.; Ghommem, M. "Turn-on" fluorescence-based diclofenac detection using metal-organic framework-coated silicon micropillars. *J. Water. Process. Eng.* **2025**, *76*, 108240. DOI
35. Goswami, A.; Ghosh, D.; Pradhan, D.; Biradha, K. *In Situ* grown Mn(II) MOF upon nickel foam acts as a robust self-supporting bifunctional electrode for overall water splitting: a bimetallic synergistic collaboration strategy. *ACS. Appl. Mater. Interfaces.* **2022**, *14*, 29722-34. DOI PubMed
36. Gourji, F. H.; Rajaramanan, T.; Kishore, A.; Heggertveit, M.; Velauthapillai, D. Hierarchical cube-in-cube cobalt-molybdenum phosphide hollow nanoboxes derived from the MOF template strategy for high-performance supercapacitors. *ACS. Omega.* **2023**, *8*, 23446-56. DOI PubMed PMC
37. Gu, X.; Ji, Y.; Tian, J.; Wu, X.; Feng, L. Combined MOF derivation and fluorination imparted efficient synergism of Fe-Co fluoride for oxygen evolution reaction. *Chem. Eng. J.* **2022**, *427*, 131576. DOI
38. Gu, Z.; Yang, C.; Chang, N.; Yan, X. Metal-organic frameworks for analytical chemistry: from sample collection to chromatographic separation. *Acc. Chem. Res.* **2012**, *45*, 734-45. DOI
39. Sahoo, S.; Rout, C. S. Facile electrochemical synthesis of porous manganese-cobalt-sulfide based ternary transition metal sulfide nanosheets architectures for high performance energy storage applications. *Electrochim. Acta.* **2016**, *220*, 57-66. DOI
40. Hong, L.; Yang, Q.; Zhang, R.; Zhao, J. A novel strategy synthesized highly specific surface area bimetallic CoMn-MOFs as electrode materials for supercapacitors. *J. Inorg. Organomet. Polym. Mater.* **2025**, *35*, 8391-403. DOI
41. Hu, Y.; Wu, Y.; Devendran, C.; et al. Preparation of nanoporous graphene oxide by nanocrystal-masked etching: toward a nacre-mimetic metal-organic framework molecular sieving membrane. *J. Mater. Chem. A.* **2017**, *5*, 16255-62. DOI
42. Avci, C.; Ariñez-Soriano, J.; Carné-Sánchez, A.; et al. Post-synthetic anisotropic wet-chemical etching of colloidal sodalite ZIF crystals. *Angew. Chem. Int. Ed.* **2015**, *54*, 14417-21. DOI PubMed PMC
43. Huang, H.; Sun, Y.; Jia, X.; et al. air-steam etched construction of hierarchically porous metal-organic frameworks. *Chin. J. Chem.* **2021**, *39*, 1538-44. DOI
44. Wang, D.; Zhu, F.; Dang, Y.; et al. Conformal phosphating hierarchical interface of CC/CoNiMn-P for hybrid supercapacitors with high cycling stability. *Inorg. Chem. Front.* **2025**, *12*, 3098-109. DOI

45. Chen, F.; Mu, X.; Zhou, J.; et al. Engineering the active sites of MOF-derived catalysts: from oxygen activation to activate metal-air batteries†. *Chin. J. Chem.* **2024**, *42*, 2520-35. DOI
46. Chen, L.; Cheng, H.; Hu, R.; et al. Kirkendall effect-mediated transformation of ZIF-67 to NiCo-LDH nanocages as oxidase mimics for multicolor point-of-care testing of β-galactosidase activity and *Escherichia coli*. *Anal. Chem.* **2025**, *97*, 2853-62. DOI
47. Wang, D.; Zhao, Z. Y.; Wang, P.; Wang, S. M.; Feng, M. Synthesis of MOF-derived nitrogen-doped carbon microtubules via template self-consumption. *Rare. Metals.* **2022**, *41*, 2582-7. DOI
48. Yin, H.; Liu, X.; Wang, L.; Isimjan, T. T.; Cai, D.; Yang, X. Real active site identification of $Co/Co_3O_4$ anchoring Ni-MOF nanosheets with fast OER kinetics for overall water splitting. *Inorg. Chem.* **2024**, *63*, 7045-52. DOI
49. Wang, P.; Yang, C.; Yao, J.; Li, H.; Hu, Z.; Li, Z. Two-dimensional metal organic framework nanosheets in electrocatalysis. *Chem. Sci.* **2025**, *16*, 6583-97. DOI PubMed PMC
50. Murugasamy, J.; Ramasundaram, S.; Mishra, N. K.; et al. Development of alkali-etched ZIF-67 metal-organic framework composite incorporated PVDF UF membranes for efficient wastewater treatment. *J. Taiwan. Inst. Chem. Eng.* **2026**, *179*, 106424. DOI
51. Zhai, H.; Zhang, G.; Zhang, Z.; et al. Ultrahigh gas response of chlorine sensor based on $In_2O_3$ multibeam pores by etching precursor MOFs with urea. *J. Environ. Chem. Eng.* **2025**, *13*, 118027. DOI
52. Lee, H. J.; Cho, W.; Oh, M. Advanced fabrication of metal-rganic frameworks: template-directed formation of polystyrene@ZIF-8 core-hell and hollow ZIF-8 microspheres. *Chem. Commun.* **2012**, *48*, 221-3. DOI
53. Song, X.; Zou, Y.; Liu, X.; Oh, M.; Lah, M. S. A two-fold interpenetrated (3,6)-connected metal-rganic framework with rutile topology showing a large solvent cavity. *New. J. Chem.* **2010**, *34*, 2396. DOI
54. Deng, L.; Liu, P.; Xiao, H.; et al. In-situ architecting hydrophilic, defect-rich MgMn-MOF on bimetallic oxide loaded biochar for smartphone-operated portable electrochemical-colorimetric dual-mode intelligent sensing of $Cu^{2+}$ in rice plants. *Sens. Actuators. B:. Chem.* **2025**, *439*, 137859. DOI
55. Ding, J.; Sun, Q.; Zhong, L.; et al. Thermal conversion of hollow nickel-organic framework into bimetallic $FeNi_3$ alloy embedded in carbon materials as efficient OER electrocatalyst. *Electrochim. Acta.* **2020**, *354*, 136716. DOI
56. Pravin, M. B. S.; Mazhar, W.; Alshamari, A.; et al. MOF-assisted synthesis of hierarchically porous ZIF-67-derived $Co_3O_4$ nanosheets enabling high specific capacitance and long-cycle stability for high-current-density supercapacitors. *J. Electron. Mater.* **2026**, *55*, 4186-201. DOI
57. Wang, Q.; Luo, J.; Wu, Y.; Xie, Y.; Cheng, L. Tunable electromagnetic response behaviors via cross-cale morphological structural engineering for ultra-ideband microwave absorption†. *Chin. J. Chem.* **2025**, *43*, 2756-70. DOI
58. Li, H.; Li, Y.; Liu, Y.; Guo, J.; Yi, Z. Hierarchical collaborative architecture of MOF-derived cobalt phosphide-porous carbon conductive networks: enabling high-performance supercapacitor energy storage. *Appl. Surf. Sci.* **2026**, *730*, 166369. DOI
59. Lei, J.; Li, S.; Zhen, X.; Shen, L.; He, B. Pr-doped NiFe-layered double hydroxide on plasma-etched nickel foam as a high-efficiency electrocatalyst for oxygen evolution reaction. *Dalton. Trans.* **2026**, *55*, 2071-9. DOI
60. Chen, M.; Jiang, Z.; Wang, R.; et al. Polymetallic Prussian blue analogues with hierarchical structure for high efficiency oxygen evolution reactions. *Int. J. Hydrogen. Energy.* **2024**, *54*, 963-70. DOI
61. Li, S.; Wu, P.; Ming, Z.; Liu, C.; Wang, W.; Chen, Z. A *de novo* sacrificial-MOF strategy for fabricating cellulose nanofibers/ZIF-8/PANI gel composite membranes for high-performance flexible supercapacitors. *Gels.* **2026**, *12*, 134. DOI PubMed PMC
62. Li, H.; Shu, C.; Chen, G.; et al. Dual-templates-assisted synthesis of hollow nanoreactors with hierarchically porous shell for efficient oxygen reduction reaction. *Fuel.* **2025**, *402*, 136058. DOI
63. Herrera-herrera, P. A.; Rodríguez-Sevilla, E.; Varela, A. S. The role of the metal center on charge transport rate in MOF-525: cobalt and nickel porphyrin. *Dalton. Trans.* **2021**, *50*, 16939-44. DOI PubMed
64. Tan Y, Chun Zeng H. Self-templating synthesis of hollow spheres of MOFs and their derived nanostructures. *Chem. Commun.* **2016**, *52*, 11591-4. DOI PubMed
65. Chen, X.; Zhang, K.; Hassan, Z. M.; Redel, E.; Baumgart, H. Charge. transport, conductivity and Seebeck coefficient in pristine and TCNQ loaded preferentially grown metal-organic framework films. *J. Phys:. Condens. Matter.* **2022**, *34*, 404001. DOI
66. Hu, H.; Xie, H.; Liang, S.; et al. Fabricating MOF-supported nonprecious metal nanocatalysts from the commercial metal dusts via a mechanochemistry-assisted sacrificial strategy. *Inorg. Chem.* **2025**, *64*, 21674-82. DOI
67. Hu, P.; Qin, H.; Hu, K.; Dai, R.; Wang, Z.; Huang, K. Constructing a defect-rich hydroxide nanoenzyme sensor based on dielectric barrier discharge microplasma etching for sensitive detection of thiamine hydrochloride and hydrogen peroxide. *J. Colloid. Interface. Sci.* **2022**, *628*, 597-606. DOI PubMed

68. Qin, H.; Dai, R.; Hu, P.; et al. Constructing a hollow-cage nanoenzyme sensor for dual detection of thiamine hydrochloride and hydrogen peroxide based on dielectric barrier discharge microplasma etching. *Microchem. J.* **2024**, *207*, 112016. DOI
69. Yu, S.; Li, C.; Zhao, S.; Chai, M.; Hou, J.; Lin, R. Recent advances in the interfacial engineering of MOF-based mixed matrix membranes for gas separation. *Nanoscale.* **2024**, *16*, 7716-33. DOI
70. Zhang, S.; Wang, C.; Meng, X.; et al. Enhanced electromagnetic wave absorption of multicore $Fe_4N$@N-doped porous carbon core-shell microspheres through dielectric-magnetic coordination. *Carbon.* **2025**, *237*, 120176. DOI
71. Liu, P.; Gao, S.; Zhang, G.; Huang, Y.; You, W.; Che, R. Hollow engineering to Co@N-doped carbon nanocages via synergistic protecting-etching strategy for ultrahigh microwave absorption. *Adv. Funct. Mater.* **2021**, *31*, 2102812. DOI
72. Li, H.; Lin, H.; Raza, S.; et al. Construction of MXene-MOF membranes with photocatalytic self-cleaning for enhanced oil-water emulsion separation. *J. Membr. Sci.* **2025**, *718*, 123685. DOI
73. Liu, W.; Huang, J.; Yang, Q.; et al. Multi-shelled hollow metal-organic frameworks. *Angew. Chem. Int. Ed.* **2017**, *56*, 5512-6. DOI
74. Park, S.; Ryu, J.; Cho, H. Y.; Sohn, D. Halloysite nanotubes loaded with HKUST-1 for $CO_2$ adsorption. *Colloid. Surface. A.* **2022**, *651*, 129750. DOI
75. Cai, Z. X.; Wang, Z. L.; Xia, Y. J.; et al. Tailored catalytic nanoframes from metal-organic frameworks by anisotropic surface modification and etching for the hydrogen evolution reaction. *Angew. Chem. Int. Ed.* **2021**, *60*, 4747-55. DOI
76. Zeng, H.; Qiu, P.; Huang, Z.; Tan, X.; Huang, Z.; Zhou, Y. Controllable synthesis and morphology engineering of S-doped NiCo layered double hydroxide nanoflowers for high-performance supercapacitors. *J. Power. Sources.* **2026**, *665*, 238966. DOI
77. Ulisso, D. M.; Mane, S. A.; Chavan, R. A.; Kamble, G. P.; Kolekar, S. S.; Ghule, A. V. Multilayered core-shell NiCo-layered double hydroxide@$NiCo_2O_4$ composite electrode for high-performance supercapacitor. *J. Alloys. Compd.* **2024**, *980*, 173563. DOI
78. Main, R. M.; Cordes, D. B.; Desai, A. V.; et al. Solvothermal synthesis of a novel calcium metal-organic framework: high temperature and electrochemical behaviour. *Molecules.* **2021**, *26*, 7048. DOI PubMed PMC
79. Deyko, G.; Kravtsov, L.; Glukhov, L.; et al. Synthesis and adsorption properties of new calcium metal-organic framework (Ca-MOF) ZIOC-10 based on a new carbazole linker. *Microporous. Mesoporous. Mater.* **2024**, *373*, 113120. DOI
80. Zheng, Y.; Hu, H.; Zhu, Y.; et al. ZIF-67-Derived (NiCo)$S_2$@NC nanosheet arrays hybrid for efficient overall water splitting. *Inorg. Chem.* **2022**, *61*, 14436-46. DOI
81. Pan, Y.; Sun, K.; Liu, S.; et al. Core-shell ZIF-8@ZIF-67-derived CoP nanoparticle-embedded N-doped carbon nanotube hollow polyhedron for efficient overall water splitting. *J. Am. Chem. Soc.* **2018**, *140*, 2610-8. DOI
82. Yi, F. Y.; Zhang, R.; Wang, H.; et al. Metal-organic frameworks and their composites: synthesis and electrochemical applications. *Small. Methods.* **2017**, *1*, 1700187. DOI
83. Guan, B. Y.; Yu, X. Y.; Wu, H. B.; Lou, X. W. Complex nanostructures from materials based on metal-organic frameworks for electrochemical energy storage and conversion. *Adv. Mater.* **2017**, *29*, 1703614. DOI PubMed
84. Lan, Y.; Yu, R.; Wang, Q.; Dai, J. Synthesis of ultra-high specific surface area trimetallic NiCoMg-LDH hollow cage via bimetallic ion etching for hybrid supercapacitors. *Ionics.* **2024**, *30*, 3033-44. DOI
85. Yu, Z.; Sun, Y.; Zhang, Z.; Geng, C.; Qiao, Z. Rational matching of metal-organic frameworks and polymers in mixed matrix membranes for efficient propylene/propane separation. *Polymers.* **2024**, *16*, 2545. DOI PubMed PMC
86. Li, H.; Sun, Y.; Guan, J.; et al. Amidoxime-functionalized PIM-1 incorporating defect-engineered ZIF-8 for enhanced propylene/propane separation and plasticization resistance. *J. Membr. Sci.* **2025**, *722*, 123907. DOI
87. Zhang, J.; Yu, L.; Chen, Y.; Lu, X. F.; Gao, S.; Lou, X. W. Designed formation of double-shelled Ni-Fe layered-double-hydroxide nanocages for efficient oxygen evolution reaction. *Adv. Mater.* **2020**, *32*, 1906432. DOI
88. Xia, W.; Tang, J.; Li, J.; et al. Defect-rich graphene nanomesh produced by thermal exfoliation of metal-organic frameworks for the oxygen reduction reaction. *Angew. Chem. Int. Ed.* **2019**, *58*, 13354-9. DOI
89. Liu, Y.; Hu, J.; Zhu, Q.; et al. Preparation of NiCo-LDH composite materials derived from NiCo-MOF by alkaline etching for high performance supercapacitor. *J. Phys. Chem. Solids.* **2025**, *206*, 112834. DOI
90. Wang, X.; Wang, M.; Chen, M.; Zhang, Y. A mini review of ceramic-based MOF membranes for water treatment. *Membranes.* **2023**, *13*, 751. DOI PubMed PMC
91. Wang, Y.; Yang, G.; Chao, M.; et al. Molten salts etching driven *in-situ* construction of MOF-derived Co/Co-N-C/MXene toward oxygen reduction catalysis. *Energy. Fuels.* **2025**, *39*, 8283-90. DOI
92. Lu, Y.; Zhou, H.; Yang, H.; Zhou, Z.; Jiang, Z.; Pang, H. Anisotropy of metal-organic framework and their composites: properties, synthesis, and applications. *J. Mater. Chem. A.* **2024**, *12*, 6243-60. DOI
93. Corma, A.; García, H.; Llabrés i Xamena, F. X. Engineering metal organic frameworks for heterogeneous catalysis. *Chem. Rev.* **2010**, *110*, 4606-55. DOI

94. Sun, W.; Zhang, X.; Zhu, H.; et al. Hollow metal-organic frameworks micro-/nanoreactors via *in-situ* cascade engineering: boosting neurotransmitter sensitive recognition. *Adv. Compos. Hybrid. Mater.* **2025**, *9*, 33. DOI
95. Lin, Z.; Guo, M.; Wang, Y.; et al. Accelerated structural transformation of metal-organic frameworks via interfacial engineering for efficient oxygen evolution reaction. *Int. J. Hydrogen. Energy.* **2024**, *85*, 766-72. DOI
96. Zhang, H.; Jiang, Q.; Hadden, J. H. L.; Xie, F.; Riley, D. J. Pd ion-exchange and ammonia etching of a Prussian blue analogue to produce a high-performance water-splitting catalyst. *Adv. Funct. Mater.* **2021**, *31*, 2008989. DOI
97. Sumida, K.; Liang, K.; Reboul, J.; Ibarra, I. A.; Furukawa, S.; Falcaro, P. Sol-gel processing of metal-organic frameworks. *Chem. Mater.* **2017**, *29*, 2626-45. DOI
98. Zhao, W.; Zeng, Y.; Zhao, Y.; Wu, X. Recent advances in metal-organic framework-based electrode materials for supercapacitors: a review. *J. Energy. Storage.* **2023**, *62*, 106934. DOI
99. Wei, T.; Lu, J.; Wang, M.; et al. MOF-derived materials enabled lithiophilic 3D hosts for lithium metal anode - a review. *Chin. J. Chem.* **2023**, *41*, 1861-74. DOI
100. Liu, F.; Zuo, P.; Li, J.; et al. A layered multifunctional framework based on polyacrylonitrile and MOF derivatives for stable lithium metal anode. *J. Energy. Chem.* **2024**, *93*, 282-8. DOI
101. Ren, Y.; Xu, Y. Three-dimensional graphene/metal-organic framework composites for electrochemical energy storage and conversion. *Chem. Commun.* **2023**, *59*, 6475-94. DOI
102. Li, X.; Feng, X.; Meng, D.; et al. Fabrication of $TiO_2$/MOF type II heterojunction by growth of $TiO_2$ on Cr-based MOF for enhanced photocatalytic hydrogen production. *Cryst. Growth. Des.* **2025**, *25*, 1182-9. DOI
103. Ren, S.; Jin, Y.; Wang, R.; Wang, T.; Chen, P. *In-situ* growth of $Li_4Ti_5O_{12}$ on MXene and self-assembly with hollow Co/C microspheres to form an ultra-broadband and high-performance microwave absorber. *Chem. Eng. J.* **2025**, *522*, 167835. DOI
104. Murugesan, A.; Li, H.; Shoaib, M. Recent advances in functionalized carbon quantum dots integrated with metal-organic frameworks: emerging platforms for sensing and food safety applications. *Foods.* **2025**, *14*, 2060. DOI PubMed PMC
105. Song, J.; Yu, Y.; Han, X.; et al. Novel MOF(Zr)-on-MOF(Ce) adsorbent for elimination of excess fluoride from aqueous solution. *J. Hazard. Mater.* **2024**, *463*, 132843. DOI
106. Yan, W.; Liao, M.; Luo, C.; Zhang, K.; Wu, G.; Zeng, H. $CoAl_2O_4$ quantum dots/CoAl-LDH mott-Schottky heterostructure for enhancing electrochemical properties in supercapacitors. *Chem. Eng. J.* **2025**, *514*, 162708. DOI
107. Narciso, J.; Ramos-Fernandez, E. V.; Delgado-Marín, J. J.; Affolter, C. W.; Olsbye, U.; Redekop, E. A. New route for the synthesis of Co-MOF from metal substrates. *Microporous. Mesoporous. Mater.* **2021**, *324*, 111310. DOI
108. Mai, J.; Zhang, Y.; He, H.; et al. Metal-support interface engineering for stable and enhanced hydrogen evolution reaction. *Mater. Today. Chem.* **2024**, *38*, 102079. DOI
109. Cao, K.; Yuan, G.; Liu, M.; Lu, S.; Shin, B.; Yu, L. Organoselenium catalyzed reaction: sustainable chemistry from laboratory to industry. *Sustainable. Engineering. Novit.* **2025**, *1*, 1. DOI
110. Guan, B. Y.; Yu, L.; Lou, X. W. General Synthesis of Multishell Mixed-Metal Oxyphosphide Particles with Enhanced Electrocatalytic Activity in the Oxygen Evolution Reaction. *Angew. Chem. Int. Ed.* **2017**, *56*, 2386-9. DOI PubMed
111. Luo, J.; Wang, X.; Wang, S.; et al. MOF-derived S-doped $NiCo_2O_4$ hollow cubic nanocage for highly efficient electrocatalytic oxygen evolution. *J. Colloid. Interface. Sci.* **2024**, *656*, 297-308. DOI
112. Hu, K.; Li, B.; Tian, Z.; Chen, L. Multiscale simulation in fuel cell and electrolyzer systems: a review of methods, applications, and future prospects. *Sustainable. Engineering. Novit.* **2025**, *1*, 5. DOI
113. Yang, Q.; Yang, C. C.; Lin, C. H.; Jiang, H. L. Metal-organic-framework-derived hollow n-doped porous carbon with ultrahigh concentrations of single Zn atoms for efficient carbon dioxide conversion. *Angew. Chem. Int. Ed.* **2019**, *58*, 3511-5. DOI PubMed
114. Yu, L.; Yang, J. F.; Lou, X. W. Formation of $CoS_2$ nanobubble hollow prisms for highly reversible lithium storage. *Angew. Chem. Int. Ed.* **2016**, *55*, 13422-6. DOI
115. Chaouiki, A.; Chafiq, M.; Ko, Y. G. The art of controlled nanoscale lattices: a review on the self-assembly of colloidal metal-organic framework particles and their multifaceted architectures. *Mat. Sci. Eng. R.* **2024**, *159*, 100785. DOI
116. Yang, J.; Zhang, F.; Lu, H.; et al. Hollow Zn/Co ZIF particles derived from core-shell ZIF-67@ZIF-8 as selective catalyst for the semi-hydrogenation of acetylene. *Angew. Chem. Int. Ed.* **2015**, *54*, 10889-93. DOI
117. Sun, L.; Yuan, Y.; Wang, F.; Zhao, Y.; Zhan, W.; Han, X. Selective wet-chemical etching to create $TiO_2$@MOF frame heterostructure for efficient photocatalytic hydrogen evolution. *Nano. Energy.* **2020**, *74*, 104909. DOI
118. Cui, Y.; Shao, Z.; Zhao, Y.; et al. Thermal steam reduction etching to construct POM@CuICuII-BTC with hierarchical porosity for adsorption property enhancement. *Chem. Eng. J.* **2022**, *450*, 137966. DOI

119. Wang, C.; Zhang, J.; Zhang, Z.; Ren, G.; Cai, D. One-step conversion of tannic acid-modified ZIF-67 into oxygen defect hollow $Co_3O_4$/nitrogen-doped carbon for efficient electrocatalytic oxygen evolution. *RSC. Adv.* **2020**, *10*, 38906-11. DOI PubMed PMC
120. Liu, Y.; Tang, C.; Cheng, M.; et al. Polyoxometalate@metal-organic framework composites as effective photocatalysts. *ACS. Catal.* **2021**, *11*, 13374-96. DOI
121. Mo, R.; Chen, S.; Huang, L.; et al. Regulating ion affinity and dehydration of metal-organic framework sub-nanochannels for high-precision ion separation. *Nat. Commun.* **2024**, *15*, 2145. DOI PubMed PMC
122. Ma, S.; Han, W.; Han, W.; Dong, F.; Tang, Z. Recent advances and future perspectives in MOF-derived single-atom catalysts and their application: a review. *J. Mater. Chem. A.* **2023**, *11*, 3315-63. DOI
123. Lyu, C.; Ding, Y.; Yu, Z.; et al. Hierarchical pore engineering and single-site synergy: in situ construction of functionalized MOF for highly active C-N coupling. *Acta. Chim. Sin.* **2026**, *84*, 119. DOI
124. Xu, H.; Shang, H.; Wang, C.; Du, Y. Low-dimensional metallic nanomaterials for advanced electrocatalysis. *Adv. Funct. Mater.* **2020**, *30*, 2006317. DOI
125. Wang, X.; Zhou, W.; Zhai, S.; et al. Metal-organic frameworks: direct synthesis by organic acid-etching and reconstruction disclosure as oxygen evolution electrocatalysts. *Angew. Chem. Int. Ed.* **2024**, *63*, e202400323. DOI
126. Lee, Y.; Bae, S.; Kim, J. W.; et al. Metal surface passivation in semiconductor processing of Mo, W, TiN/TiSiN, and Cu: emerging strategies for corrosion and etching control. *Materials. &. Design.* **2026**, *263*, 115650. DOI
127. Wang, Q.; Astruc, D. State of the art and prospects in metal-organic framework (MOF)-based and MOF-derived nanocatalysis. *Chem. Rev.* **2020**, *120*, 1438-511. DOI PubMed
128. Zhou, C.; Cui, W.; Cui, S.; Li, G.; Han, L. MOF-derived Co(Fe)OOH slab and Co/MoN nanosheet-covered hollow-slab for efficient overall water splitting. *ACS. Appl. Mater. Interfaces.* **2024**, *16*, 69368-78. DOI
129. Farooq, A.; Zafar, F.; Ul, Hassan. S.; et al. Rational design of metal-organic framework hybrids via metal and ligand engineering for enhanced oxygen evolution reaction catalysis. *Energy. Fuels.* **2025**, *39*, 23796-804. DOI
130. Zhang, Z.; Han, L.; Tao, K. $MnO_x$-decorated MOF-derived nickel-cobalt bimetallic phosphide nanosheet arrays for overall water splitting. *Dalton. Trans.* **2024**, *53*, 1757-65. DOI
131. Li, S.; Ma, C.; Hou, J.; et al. Highly porous metal-organic framework glass design and application for gas separation membranes. *Nat. Commun.* **2025**, *16*, 1622. DOI PubMed PMC
132. Li, B.; Li, Q.; Yang, S.; He, J.; Mi, Y.; Du, P. Controlled ion-etching synthesis of MOF-derived rattle-type nickel hydroxide nanostructures for enhanced electrochemical performance in supercapacitors. *Electrochim. Acta.* **2025**, *542*, 147514. DOI
133. Zhang, Y.; Lu, J. D.; Zhang, G. X.; Zhu, R. M.; Pang, H. Ternary alloy and metal oxides embedded in yolk-shell polyhedrons as bifunctional oxygen electrocatalyst. *Rare. Metals.* **2024**, *43*, 478-88. DOI
134. Peng, B.; She, H.; Wei, Z.; et al. Sulfur-doping tunes p-d orbital coupling over asymmetric Zn-Sn dual-atom for boosting $CO_2$ electroreduction to formate. *Nat. Commun.* **2025**, *16*, 2217. DOI PubMed PMC
135. He, P.; Yu, X. Y.; Lou, X. W. Carbon-incorporated nickel-cobalt mixed metal phosphide nanoboxes with enhanced electrocatalytic activity for oxygen evolution. *Angew. Chem. Int. Ed.* **2017**, *56*, 3897-900. DOI PubMed
136. Zhu, R.; Zhang, Y.; Liu, L.; Li, Y.; He, G.; Pang, H. Bimetal-doped cobalt oxyhydroxides/hydroxides synthesized by electrochemistry for enhanced OER activity. *Inorg. Chem. Front.* **2024**, *11*, 5449-57. DOI
137. Liu, T.; Zhang, L.; Cheng, B.; Yu, J. Hollow carbon spheres and their hybrid nanomaterials in electrochemical energy storage. *Adv. Energy. Mater.* **2019**, *9*, 1803900. DOI
138. Al-Aoh, H. A.; Panneerselvam, C.; Alghamdi, A. M.; Alasmari, A.; Mohammedsaleh, Z. M. Recent advances in MXene nanozymes: synthesis, surface modifications, catalytic properties, and their emerging roles in biosensing and therapeutic applications. *Analyst.* **2026**, *151*, 991-1007. DOI PubMed
139. Wang, X.; Yang, L.; Xing, C.; et al. MOF-derived ultrathin cobalt molybdenum phosphide nanosheets for efficient electrochemical overall water splitting. *Nanomaterials.* **2022**, *12*, 1098. DOI PubMed PMC
140. Zhang, M.; Shan, Y.; Kong, Q.; Pang, H. Applications of metal-organic framework-graphene composite materials in electrochemical energy storage. *FlatChem.* **2022**, *32*, 100332. DOI
141. Ali, A.; Ahmed, S.; Jiang, W.; Park, G.; Oh, S. J. Harnessing MOF intrinsic properties for enhanced supercapacitor performance. *Curr. Opin. Electrochem.* **2025**, *50*, 101640. DOI
142. Han, D.; Wang, P.; Dang, Y.; et al. Facile electrochemical conversion strategy for fabricating cobalt-based double metal sulfide nanosheets with high capacity and low electrochemical impedance. *J. Alloys. Compd.* **2024**, *1007*, 176401. DOI
143. Wang, S.; Niu, M.; Zheng, J.; et al. Hollow porous cop-carbon nanocages for hydrogen evolution reactions. *ACS. Appl. Nano. Mater.* **2024**, *7*, 12821-9. DOI
144. Li, X.; Ye, G.; Zhu, W.; et al. Directional construction of low-coordination Fe-$N_3$ coupled with intrinsic carbon defects for high-efficiency oxygen reduction. *ACS. Nano.* **2024**, *18*, 24505-14. DOI
145. Husain, A.; Lee, D.; Siddiqui, Q. T.; Gunnasegaran, P.; Danish, M.; Jo, W. Scalable integration of MOFs, COFs, and MXenes with g-$C_3N_4$ for solar $H_2$ generation: a review of energy conversion strategies. *Int. J. Hydrogen. Energy.* **2025**, *150*, 150041. DOI

146. Kim, H.; Lah, M. S. Templated and template-free fabrication strategies for zero-dimensional hollow MOF superstructures. *Dalton. Trans.* **2017**, *46*, 6146-58. DOI PubMed
147. Yang, Y.; Yang, Y.; Zhang, X.; et al. A hierarchically porous MOF engineered via chelation-etching for high-capacity selective dye adsorption. *J. Solid. State. Chem.* **2025**, *352*, 125609. DOI
148. Liao, X.; Fu, H.; Yan, T.; Lei, J. Electroactive metal-organic framework composites: design and biosensing application. *Biosens. Bioelectron.* **2019**, *146*, 111743. DOI
149. Tuan, D. D.; Khiem, C.; Kwon, E.; et al. Hollow porous cobalt oxide nanobox as an enhanced for activating monopersulfate to degrade 2-hydroxybenzoic acid in water. *Chemosphere.* **2022**, *294*, 133441. DOI
150. Tang, X.; Li, N.; Pang, H. Metal-organic frameworks-derived metal phosphides for electrochemistry application. *Green. Energy. &. Environment.* **2022**, *7*, 636-61. DOI
151. Zhao, Z.; Duan, H.; Pang, H.; Zhu, R. A hierarchically porous ZIF@LDH core-shell structure for high-performance supercapacitors. *Chem-Asian. J.* **2021**, *16*, 845-9. DOI
152. Liu, J.; Lv, S.; Gong, Y.; et al. Water-etched approach to hierarchically porous metal-organic frameworks with high stability. *Inorg. Chem.* **2023**, *62*, 11611-7. DOI
153. Hu, A.; Pang, Q.; Tang, C.; et al. Epitaxial growth and integration of insulating metal-organic frameworks in electrochemistry. *J. Am. Chem. Soc.* **2019**, *141*, 11322-7. DOI
154. Sun, X.; Li, X.; Chen, P.; Zhu, Y. Controllable regulation of defects in nitrogen-doped hollow core-shell magnetoelectric microspheres towards preferable electromagnetic absorption. *Carbon.* **2025**, *234*, 119963. DOI
155. Xu, S.; Huang, Q.; Xue, J.; et al. Morphologically controlled metal-organic framework-derived feni oxides for efficient water oxidation. *Inorg. Chem.* **2022**, *61*, 8909-19. DOI
156. Lu, Y.; Yu, L.; Wu, M.; Wang, Y.; Lou, X. W. Construction of Complex $Co_3O_4$@$Co_3V_2O_8$ Hollow structures from metal-organic frameworks with enhanced lithium storage properties. *Adv. Mater.* **2017**, *30*, 1702875. DOI
157. Mukherjee, P.; Sathiyan, K.; Higashimine, K.; Khoshsefat, M.; Manchan, R. P.; Taniike, T. Surface engineering approach to maximize the potential of Prussian blue analog nanostructures for electroreduction of $CO_2$. *ACS. Appl. Nano. Mater.* **2026**, *9*, 4171-83. DOI
158. Wang, M.; Zi, Y.; Zhu, J.; Huang, W.; Zhang, Z.; Zhang, H. Construction of super-hydrophobic PDMS@MOF@Cu mesh for reduced drag, anti-fouling and self-cleaning towards marine vehicle applications. *Chem. Eng. J.* **2021**, *417*, 129265. DOI
159. Li, M.; Zhang, G.; Boakye, A.; Chai, H.; Qu, L.; Zhang, X. Recent advances in metal-organic framework-based electrochemical biosensing applications. *Front. Bioeng. Biotechnol.* **2021**, *9*, 797067. DOI PubMed PMC
160. Shin, S.; Yoon, H.; Yoon, Y.; Park, S.; Shin, M. W. Porosity tailoring of the Zn-MOF-5 derived carbon materials and its effects on the performance as a cathode for lithium-air batteries. *Microporous. Mesoporous. Mater.* **2021**, *311*, 110726. DOI
161. Sun, H.; Tang, B.; Wu, P. Hydrophilic hollow zeolitic imidazolate framework-8 modified ultrafiltration membranes with significantly enhanced water separation properties. *J. Membr. Sci.* **2018**, *551*, 283-93. DOI
162. Sun, Y.; Wang, Y.; Liu, D.; et al. $MoS_2$-coated MOF-derived hollow heterostructures for electromagnetic wave absorption. *ACS. Appl. Mater. Interfaces.* **2025**, *17*, 14278-90. DOI
163. Lin, Y.; Wang, T.; Liu, Y.; et al. Multi-nanozyme cascade system for boosting colorimetric sensing by selective etching bimetallic MOFs. *Anal. Chim. Acta.* **2025**, *1353*, 343976. DOI
164. Wang, L.; Liu, Z.; Ma, Y.; et al. Synergistic design of a semi-hollow core–shell structure and a metal–organic framework-derived Co/Zn selenide coated with MXene for high-performance lithium–sulfur batteries. *Dalton. Trans.* **2024**, *53*, 572-81. DOI
165. Liu, S.; Lu, J.; Yu, X.; Pang, H.; Zhang, Q.; Park, H. S. Rational design of metal-organic framework-nanoparticle composite electrocatalysts for sustainable nitrogen electrochemistry. *eScience.* **2025**, *5*, 100378. DOI
166. Liu, M.; Li, Q.; Xiao, X.; et al. Constructing Co-O-Ce bridge in Mott-Schottky Co/$CeO_2$ heterojunctions facilitates oxygen electrocatalysis bifunctionality for rechargeable Zn-air batteries. *J. Energy. Chem.* **2026**, *112*, 572-83. DOI
167. Li, H.; Wang, H.; Li, M.; Yan, X.; Li, H. Hierarchical MOFs with spatially ordered cascade enzymes for sensitive nitrite immunosensing. *Biosens. Bioelectron.* **2026**, *303*, 118550. DOI
168. Liu, C.; Wang, J.; Wan, J.; Yu, C. MOF-on-MOF hybrids: synthesis and applications. *Coord. Chem. Rev.* **2021**, *432*, 213743. DOI
169. Horcajada, P.; Serre, C.; Vallet-regí, M.; Sebban, M.; Taulelle, F.; Férey, G. Metal-organic frameworks as efficient materials for drug delivery. *Angew. Chem. Int. Ed.* **2006**, *45*, 5974-8. DOI PubMed
170. Zhang, L.; Li, H.; Sheng, T.; et al. Synthesizing Cu-doped $CoSe_2$ nanoframe cubics for Na-ion batteries electrodes. *Colloid. Surface. A.* **2021**, *628*, 127379. DOI
171. Yang, Y.; Xu, D.; Lyu, L.; et al. Synthesis of MOF-derived $Fe_7S_8$/C rod-like composites by controlled proportion of carbon for highly efficient electromagnetic wave absorption. *Compos. Part. A-Appl. S.* **2021**, *142*, 106246. DOI
172. Zeng, M.; Chai, Z.; Deng, X.; et al. Core-shell CdS@ZIF-8 structures for improved selectivity in photocatalytic $H_2$ generation from formic acid. *Nano. Res.* **2016**, *9*, 2729-34. DOI